4. G. J. Kubas, *Chem. Rev.* **107**, 4152 (2007).
5. J. W. Tye, M. B. Hall, M. Y. Darensbourg, *Proc. Natl. Acad. Sci. U.S.A.* **102**, 16911 (2005).
6. S. Ogo *et al*., *Science* **316**, 585 (2007).
7. S. Ogo, *Chem. Commun.* **2009**, 3317 (2009).
8. Materials and methods and spectroscopic and mass spectrometric data are available on *Science* Online.
9. Y. Higuchi, H. Ogata, K. Miki, N. Yasuoka, T. Yagi, *Structure* **7**, 549 (1999).
10. B. E. Barton, C. M. Whaley, T. B. Rauchfuss, D. L. Gray, *J. Am. Chem. Soc.* **131**, 6942 (2009).

Acknowledgments: This work was supported by the WPI; grants-in-aid 23655053, 24750058, and 24109016 (Scientific Research on Innovative Areas "Stimuli-responsive Chemical Species") from the Ministry of Education, Culture, Sports, Science and Technology (MEXT), Japan; and the Basic Research Programs CREST Type, "Development of the Foundation for Nano-Interface Technology" from JST, Japan. Crystallographic data for [**1**]$(BPh_4)_2$, [**2**](BPh_4), and $[Ni^{II}(X')Fe^{II}(Br)_2]$ have been deposited with the Cambridge Crystallographic Data Center under reference numbers CCDC-904876 (x-ray diffraction, **1**), 904877 (x-ray diffraction, **2**), 904874 (neutron scattering, **2**), and 904875 {x-ray diffraction, $[Ni^{II}(X')Fe^{II}(Br)_2]$}, respectively.

Supplementary Materials
www.sciencemag.org/cgi/content/full/339/6120/682/DC1
Materials and Methods
Figs. S1 to S12
References (*11*–*21*)

10 October 2012; accepted 27 November 2012
10.1126/science.1231345

Time Scales of Critical Events Around the Cretaceous-Paleogene Boundary

Paul R. Renne,[1,2]* Alan L. Deino,[1]† Frederik J. Hilgen,[3]† Klaudia F. Kuiper,[4]† Darren F. Mark,[5]† William S. Mitchell III,[2,6]† Leah E. Morgan,[5]† Roland Mundil,[1]† Jan Smit[4]†

Mass extinctions manifest in Earth's geologic record were turning points in biotic evolution. We present $^{40}Ar/^{39}Ar$ data that establish synchrony between the Cretaceous-Paleogene boundary and associated mass extinctions with the Chicxulub bolide impact to within 32,000 years. Perturbation of the atmospheric carbon cycle at the boundary likely lasted less than 5000 years, exhibiting a recovery time scale two to three orders of magnitude shorter than that of the major ocean basins. Low-diversity mammalian fauna in the western Williston Basin persisted for as little as 20,000 years after the impact. The Chicxulub impact likely triggered a state shift of ecosystems already under near-critical stress.

The mass extinction at the boundary (KPB) between the Cretaceous and Paleogene periods, ~66 million years ago (Ma), likely involved the catastrophic effects of a bolide impact (*1*), although other factors may have played an important role (*2*–*5*). To a large extent, ambiguity between the possible causes stems from inadequate age resolution of relevant events near KPB time. Existing geochronologic data surrounding the linkage between the KPB and the Chicxulub structure in the northern Yucatán Peninsula of Mexico actually exclude synchrony, indicating that the Chicxulub impact and cogenetic impact melt droplets, termed "tektites" (*6*–*8*), postdated the KPB by 183 ± 65 (*9*) thousand years (ky) and 181 ± 71 ky, respectively (see supplementary materials). In contrast, some data suggest that the Chicxulub impact predated the KPB by several hundred thousand years, and that discrete tektite-bearing horizons in the Gulf of Mexico region were derived from multiple impact events (*10*).

We acquired high-precision $^{40}Ar/^{39}Ar$ data to clarify these temporal relationships and thereby facilitate a clearer sequencing of events associated with the KPB extinctions and subsequent ecosystem recovery. We analyzed multiple samples of the tektites to refine the age of the Chicxulub impact, and of bentonites (altered volcanic ashes; Fig. 1) clearly associated with the KPB to test for synchrony of the boundary with the impact. $^{40}Ar/^{39}Ar$ ages (Figs. 2 and 3) were determined (see supplementary materials) by incremental heating of 14 tektites from Beloc, Haiti, giving a weighted mean age of 66.032 ± 0.058/0.072 Ma (*11*) that is indistinguishable from that determined by previous studies (*12*, *13*) when normalized to the same calibration. Combining all data yields an age of 66.038 ± 0.025/0.049 Ma for the tektites.

We also performed $^{40}Ar/^{39}Ar$ dating on sanidine separated from four bentonites in three distinct coal beds within two widely separated stratigraphic sections in the Hell Creek region of northeastern Montana. Extensive studies in this region have documented faunal, floral, and chemostratigraphic aspects of latest Cretaceous through early Paleogene terrestrial strata. Both sections contain well-documented Ir anomalies coincident with the biostratigraphically defined KPB (Fig. 1). In the Hauso Flats section, we analyzed samples from two localities ~200 m apart of a bentonite from the IrZ coal, located stratigraphically only a few centimeters above the horizon yielding the largest iridium anomaly [up to 11.7 parts per billion (ppb) at the nearby Herpijunk locality; (*14*)] reported from this area and 5 cm above the highest occurrence of Cretaceous pollen in the section (*15*). All of our data combined yield a weighted mean age of 66.043 ± 0.011/0.043 Ma. A bentonite from the Hauso Flats Z (HFZ) coal, 18 m stratigraphically above the IrZ coal, yielded an age of 65.990 ± 0.032/0.053 Ma. Isotope dilution–thermal ionization mass spectrometry (ID-TIMS) U-Pb analyses of 15 chemically abraded zircons from the same HFZ coal bentonite yielded a weighted mean age of 65.988 ± 0.074 Ma, in agreement with the $^{40}Ar/^{39}Ar$ results. In the Hell Creek Marina road section, we analyzed two bentonites within the Z coal, which lies 50 to 60 cm above a 0.57-ppb Ir anomaly (*16*). The two bentonites are separated stratigraphically by ~30 cm and yield results for the lower (Z_2) and upper (Z_1) bentonites of 66.019 ± 0.021/0.046 Ma and 66.003 ± 0.033/0.053 Ma, respectively.

The IrZ coal bentonite is much closer stratigraphically to both impact signals and the biostratigraphically defined KPB than the Z coal bentonites; thus, it should be regarded as the closest stratigraphic proxy for the KPB. Accordingly, a comparison with the pooled age for the Beloc tektites indicates a statistically insignificant age difference of 5 ± 27 ky between the two events. Thus, the hypothesis that the Chicxulub impact predated the KPB by ~300 ky (*10*) is unsupported by our data. Our preferred absolute age for the KPB, including propagated systematic uncertainties, is 66.043 ± 0.043 Ma. This age, which is intrinsically calibrated by both ^{40}K and ^{238}U decay constants (*17*), is sufficiently precise to discriminate between 100-ky orbital eccentricity cycles at 66 Ma, in principle allowing comparison with astronomical tuning approaches to dating the KPB. However, the uncertainty in the astronomical solution (~40,000 years ago) at 66 Ma (*18*) effectively limits this discrimination because the 100-ky cycle is not reliable in the solution due to chaotic behavior of the solar system. Our age for the KPB, if based on the Kuiper *et al*. (*19*) calibration, would be 65.836 ± 0.061 Ma, which would be sufficiently precise to discriminate between 405-ky but not 100-ky orbital cycles. Because circum-KPB marine records generally lack appropriate materials for high-resolution radioisotopic dating, astronomical tuning potentially represents the best means of temporally calibrating marine records and enabling their comparison with terrestrial records in this time interval. A fully calibrated astronomical solution can potentially enable deconvolution of orbital forcing from other causes of climate change.

The KPB age as determined by our data for the IrZ coal bentonite agrees with the astronomical age (66 ± 0.07 Ma; option 2) derived

[1]Berkeley Geochronology Center (BGC), 2455 Ridge Road, Berkeley, CA 94709, USA. [2]Department of Earth and Planetary Science, University of California, Berkeley, CA, 94720, USA. [3]Faculty of Geosciences, Department of Earth Sciences, Utrecht University, Budapestlaan 4, 3584 CD Utrecht, Netherlands. [4]Faculty of Earth and Life Sciences, Institute of Earth Sciences,Vrije Universiteit Amsterdam, De Boelelaan 1085, 1081 HV Amsterdam, Netherlands. [5]Scottish Universities Environmental Research Centre, Rankine Avenue, East Kilbride, G75 0QF, UK. [6]Department of Chemistry, University of California, Berkeley, CA, 94720, USA.

*To whom correspondence should be addressed. E-mail: prenne@bgc.org
†These authors contributed equally to this work.

Downloaded from www.sciencemag.org on February 9, 2013

from deep-sea cores (*20*) and the preferred astronomical age (65.957 ± 0.040 Ma) inferred by Kuiper *et al*. (*19*) from the Zumaia section of Spain, but not with that (65.25 ± 0.06 Ma) of Westerhold *et al*. (*21*) (fig. S6). We conclude that the younger age inferred by Westerhold *et al*. (*21*) is a consequence of miscalibration by two 405-ky eccentricity cycles (see supplementary materials) and that the terrestrial and marine Ir anomalies are synchronous. This conclusion is strengthened by our concordant U-Pb and $^{40}Ar/^{39}Ar$ dates for the HFZ coal, which indicate that the KPB is older than 65.988 ± 0.074 Ma and 65.990 ± 0.053 Ma, respectively.

Our data indicate that the stratigraphic interval of ~18 m between the IrZ and HFZ coals in the Hauso Flats section corresponds to a duration of 53 ± 34 ky, whereas the previous $^{40}Ar/^{39}Ar$ data from the same section (*15*) suggested a duration of 390 ± 70 ky. This interval spans most of the Pu1 basal Puercan (North American Land Mammal Age) mammalian fauna known from northeastern Montana and adjacent areas in Canada, containing only 15 recognized species compared with 27 in the preceding (pre-KPB) Lancian stage (*22*). The brevity of the IrZ-HFZ interval of the basal Tullock Formation implied by our new data indicates that the depauperate Pu1 fauna persisted as briefly as 20 ky and supports the hypothesis (*22*) that much of the post-KPB vertebrate faunal recovery in the Hell Creek area occurred by immigration rather than evolutionary radiation, given that the duration of speciation events for mammals (at least, late Cenozoic ones) typically exceeds hundreds of thousands of years (*23*).

Our dating of the IrZ and HFZ bentonites constrains the terrestrial, hence atmospheric, –1.5 per mil (‰) $\delta^{13}C$ isotope anomaly in the Hauso Flats section (*24*) to have occurred early within the first 53 ± 34 ky of the Paleogene. Scaling the sediment accumulation rate by linear interpolation between the two dated horizons and allowing the maximum possible stratigraphic extent of the anomaly (considering sample interval) yield a maximum duration of 5 ± 3 ky for the anomaly. Similarly, applying our date for the IrZ bentonite to the iridium anomaly and scaling to the Z_2 bentonite in the Hell Creek Marina road section (*24*) yields a maximum duration of 13 ±13 ky for the –2.0‰ $\delta^{13}C$ anomaly there.

The terrestrial $\delta^{13}C$ anomaly is markedly consistent in magnitude, timing, and rapidity of onset with marine records, although the latter commonly show much longer recovery time scales. Some marine records [e.g., (*1*)] show an initial decrease of 1 to 2‰ followed by a rapid increase of ~1‰ on the time scale of several thousand years, succeeded by a much more gradual increase over several million years to pre-KPB values. Other cases show more rapid recovery of marine $\delta^{13}C$ to pre-KPB values, as in the Agost section of southern Spain, where the duration of the anomaly and partial recovery are estimated to have occurred over 3 to 5 ky, and full recovery to have occurred over <100 ky (*25*). Differences between $\delta^{13}C$ values in planktic versus benthic foraminifera from Atlantic and Pacific cores also show precipitous drops at the KPB, interpreted to reflect a major disruption in mixing between surface- and deep-water masses (*26*). Restoration of pre-KPB values of the differential, hence of normal ocean circulation, experienced a protracted recovery spanning several millions of years and was likely the rate-limiting determinant in recovery of general marine productivity (*26*).

Our results strengthen conclusions that the Chicxulub impact played an important role in the mass extinctions. However, global climate instability preceded the KPB (and thus, in view of our data, the Chicxulub impact) by ~1 million years (My) (*27*–*29*). During this interval, six abrupt shifts of >2°C in continental mean annual temperatures have been inferred from paleoflora in North Dakota (*29*). The most dramatic of these temperature oscillations, a drop of 6° to 8°C, occurred <100 ky before the KPB (*29*) and was closely synchronous with notable mammalian turnover in the Hell Creek area (*30*). Several cycles of latest Cretaceous sea-level oscillations are recorded in the Williston basin with an overall regression peaking just before the KPB (*31*), possibly a glacio-eustatic response to climatic cooling. Cooling at this time is consistent with a global sea-level drop of ~40 m beginning in geomagnetic polarity chron 30n and ending in chron 28r (*32*), clearly spanning the KPB. This event followed closely on a sharp sea-level drop and subsequent rise of ~30 m, coincident with the highest $\delta^{18}O$ values recorded for the 30 My before or afterward, which occurred in the middle of chron 30n (*32*), ~1 My before the KPB. Recognition of these and other relatively brief events led Miller *et al*. (*32*) to infer the existence of multiple ephemeral Antarctic ice sheets between 100 and 33 Ma.

We suggest that the brief cold snaps in the latest Cretaceous, though not necessarily of extraordinary magnitude, were particularly stressful to a global ecosystem that was well adapted to the long-lived preceding Cretaceous hothouse climate. The Chicxulub impact then provided a decisive blow to ecosystems thus already under critical stress, and in essence pushed the global ecosystem across a threshold that triggered a planetary state shift (*33*, *34*). Although the atmospheric carbon cycle was disrupted only briefly, and initial mammalian faunal changes after the KPB may have been dominated by migration, some changes such as the disappearance

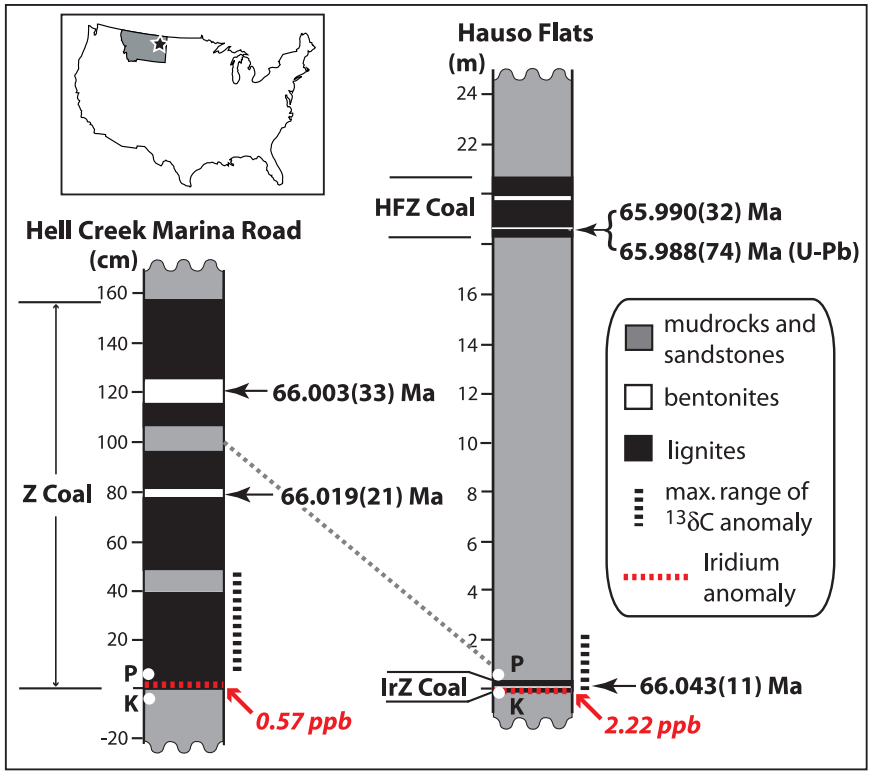

Fig. 1. Stratigraphic sections in the Hell Creek area of northeastern Montana (**inset**) showing positions of dated bentonites in relation to Ir anomalies (*16*, *41*) and carbon isotope records (*24*) from the same sections. The two sections have different vertical scales; thin dotted line connects horizons at 1 m above the Ir anomaly in the two sections. Ages shown are from $^{40}Ar/^{39}Ar$ analysis of sanidine except one (U/Pb) from U-Pb analysis of zircon. Age uncertainties (in parentheses) refer to last significant figures shown and include analytical sources only. White dots labeled P and K on both sections show the lowest occurrence of Paleocene pollen and the highest occurrence of Cretaceous pollen, respectively (*15*).

Downloaded from www.sciencemag.org on February 9, 2013

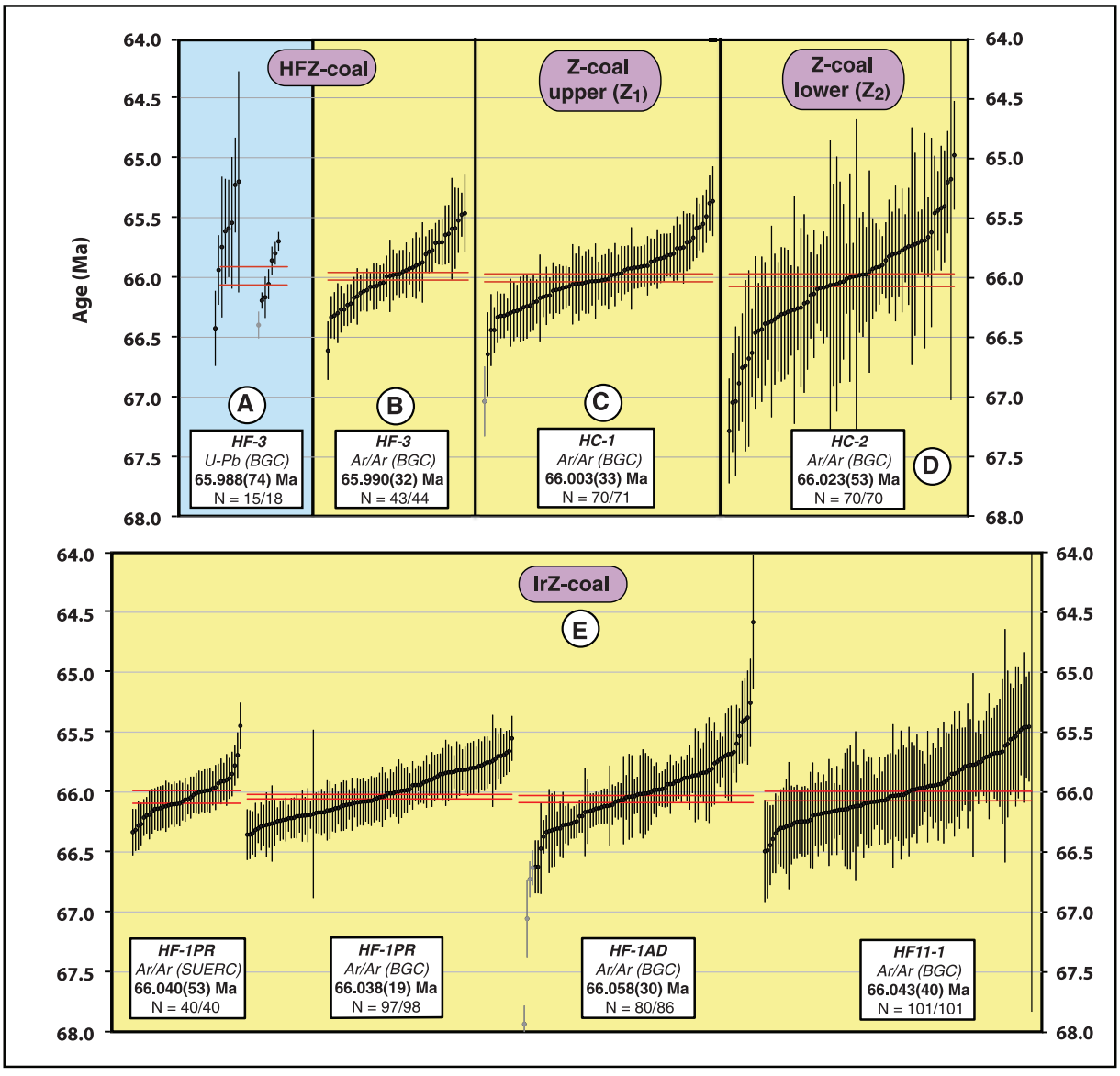

Fig. 2. Summary of single-crystal geochronology results for volcanic ashes whose stratigraphic relations are shown in Fig. 1. Individual ages are shown in ranked order with 1σ analytical uncertainty limits. Samples interpreted as xenocrysts are shown in gray and are excluded from age calculations. Uncertainty limits for the weighted mean age for each sample are shown by red lines. U-Pb results for zircon crystals (**A**) and $^{40}Ar/^{39}Ar$ results for sanidine (**B**) from an ash in the Hauso Flats Z (HFZ) coal, 18 m above the KPB, yield indistinguishable results. Two ashes in the Z-coal in the Hell Creek marina road section (**C** and **D**) yield ages consistent with stratigraphic order although they are mutually indistinguishable at 68% confidence. Four independent data sets, from three irradiations and two labs, for the IrZ coal bentonite (**E**) yield consistent results.

Fig. 3. Summary of incremental heating $^{40}Ar/^{39}Ar$ age (lower panels) and Ca-K composition data (upper panels) for (**A**) fourteen tektites from Beloc, Haiti, and multgrained feldspar samples from the IrZ (**B**) and Z_2 (**C**) bentonites shown in Fig. 1.

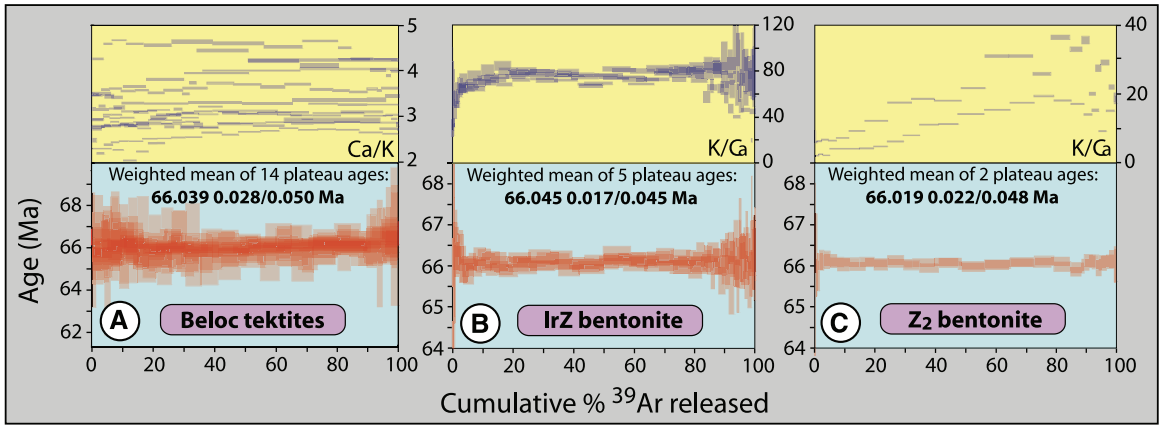

Downloaded from www.sciencemag.org on February 9, 2013

of nonavian dinosaurs were permanent. Thus, whereas some paleoenvironments may have been restored relatively rapidly, terrestrial and marine ecosystems changed forever.

The cause of the precursory climate perturbations that pushed some ecosystems to the tipping point is unclear, but a leading candidate is volcanogenic volatile emissions (*35*) from early pulses of the episodically erupted Deccan Traps (*36*, *37*). The magmatic event producing the Deccan Traps was clearly initiated prior to the KPB (*38*), and the most voluminous middle pulse of volcanism may be linked to either (i) the inception of a two-staged decline in marine $^{187}Os/^{188}Os$ beginning about 300 ky before the KPB (*39*) or (ii) the KPB itself (*36*, *37*, *40*). Existing geochronological data are insufficiently precise to constrain these relationships with age resolution comparable to that presented here for the KPB and the Chicxulub impact. Refining the timing and tempo of Deccan volcanism remains a considerable challenge whose resolution is key to evaluating the role of this event in the causes of biotic and environmental change at the KPB.

References and Notes

1. P. Schulte *et al.*, *Science* **327**, 1214 (2010).
2. J. D. Archibald *et al.*, *Science* **328**, 973, author reply 975 (2010).
3. V. Courtillot, F. Fluteau, *Science* **328**, 973, author reply 975 (2010).
4. G. Keller *et al.*, *Science* **328**, 974, author reply 975 (2010).
5. N. C. Arens, I. D. West, *Paleobiology* **34**, 456 (2008).
6. H. Sigurdsson *et al.*, *Nature* **353**, 839 (1991).
7. F. J. Maurrasse, G. Sen, *Science* **252**, 1690 (1991).
8. A. R. Hildebrand *et al.*, *Geology* **19**, 867 (1991).
9. Uncertainties here and throughout are stated at the 68% confidence level.
10. G. Keller *et al.*, *Earth Planet. Sci. Lett.* **255**, 339 (2007).
11. Uncertainties given as ±*X*/*Y* refer to values excluding (X) and including (Y) systematic sources as defined in the supplementary materials.
12. C. C. Swisher III *et al.*, *Science* **257**, 954 (1992).
13. G. B. Dalrymple, G. A. Izett, L. W. Snee, J. D. Obradovich, *U.S. Geol. Surv. Bull.* **2065**, 1 (1993).
14. J. Smit, S. van der Kaars, *Science* **223**, 1177 (1984).
15. C. C. Swisher III, L. Dingus, R. F. Butler, *Can. J. Earth Sci.* **30**, 1981 (1993).
16. H. Baadsgaard, J. F. Lerbekmo, I. McDougall, *Can. J. Earth Sci.* **25**, 1088 (1988).
17. P. R. Renne, G. Balco, K. R. Ludwig, R. Mundil, K. Min, *Geochim. Cosmochim. Acta* **75**, 5097 (2011).
18. J. Laskar *et al.*, *Astron. Astrophys.* **428**, 261 (2004).
19. K. F. Kuiper *et al.*, *Science* **320**, 500 (2008).
20. D. Husson *et al.*, *Earth Planet. Sci. Lett.* **305**, 328 (2011).
21. T. Westerhold, U. Rohl, J. Laskar, *Geochem. Geophys. Geosyst.* **13**, Q06015 (2012).
22. W. A. Clemens, in *The Hell Creek Formation and the Cretaceous-Tertiary Boundary in the Northern Great Plains: An Integrated Continental Record of the End of the Cretaceous*, J. H. Hartman, K. R. Johnson, D. J. Nichols, Eds. (Geological Society of America, Boulder, CO, 2002), vol. 361, pp. 217–245.
23. J. C. Avise, D. Walker, G. C. Johns, *Proc. R. Soc. Lond. B Biol. Sci.* **265**, 1707 (1998).
24. N. C. Arens, A. H. Jahren, *Palaios* **15**, 314 (2000).
25. J. Smit, *Geol. Mijnb.* **69**, 187 (1990).
26. S. D'Hondt, *Annu. Rev. Ecol. Evol. Syst.* **36**, 295 (2005).
27. L. Q. Li, G. Keller, *Mar. Micropaleontol.* **33**, 55 (1998).
28. E. Barrera, S. M. Savin, in *Evolution of the Cretaceous Ocean-Climate System*, E. Barrera, C. C. Johnson, Eds. (Geological Society of America, Boulder, CO, 1999), vol. 332, pp. 245–282.
29. P. Wilf, K. R. Johnson, B. T. Huber, *Proc. Natl. Acad. Sci. U.S.A.* **100**, 599 (2003).
30. G. P. Wilson, *J. Mamm. Evol.* **12**, 53 (2005).
31. E. C. Murphy, J. W. Hoganson, K. R. Johnson, in *The Hell Creek Formation and the Cretaceous-Tertiary Boundary in the Northern Great Plains: An Integrated Continental Record of the End of the Cretaceous*, J. H. Hartman, K. R. Johnson, D. J. Nichols, Eds. (Geological Society of America, Boulder, CO, 2002), pp. 9–34.
32. K. G. Miller *et al.*, *Science* **310**, 1293 (2005).
33. A. D. Barnosky *et al.*, *Nature* **486**, 52 (2012).
34. M. Scheffer *et al.*, *Nature* **461**, 53 (2009).
35. S. Self, *Philos. Trans. R. Soc. Lond. A* **364**, 2073 (2006).
36. A. L. Chenet *et al.*, *J. Geophys. Res. Solid Earth* **114**, B06103 (2009).
37. G. Keller, *Cretac. Res.* **29**, 754 (2008).
38. V. E. Courtillot, P. R. Renne, *C. R. Geosci.* **335**, 113 (2003).
39. N. Robinson, G. Ravizza, R. Coccioni, B. Peucker-Ehrenbrink, R. Norris, *Earth Planet. Sci. Lett.* **281**, 159 (2009).
40. T. S. Tobin *et al.*, *Palaeogeogr. Palaeoclimatol. Palaeoecol.* **350–352**, 180 (2012).
41. L. W. Alvarez, *Proc. Natl. Acad. Sci. U.S.A.* **80**, 627 (1983).

Acknowledgments: We thank the Ann and Gordon Getty Foundation, U.C. Berkeley's Esper S. Larsen Jr. Fund, and NSF (grants EAR 0844098 and EAR 0451802) for support of B.G.C.'s work; the Natural Environment Research Council for continued funding of the Argon Isotope Facility at the Scottish Universities Environmental Research Centre; the GTSNext project of the Marie Curie Foundation; the Marie Curie Fellowship program for support of L.E.M.; the Netherlands Organisation for Scientific Research (grant 863.07.009) for support of K.F.K.; F. Maurrasse for providing the tektites; W. Alvarez, A. Barnosky, W. Clemens, T. White, and G. Wilson for discussion and comments on the manuscript; and three anonymous reviewers for helpful suggestions. Data are available in the supplementary materials.

Supplementary Materials

www.sciencemag.org/cgi/content/full/339/6120/684/DC1
Materials and Methods
Supplementary Text
Figs. S1 to S7
Tables S1 to S4
References (*42*–*66*)

20 September 2012; accepted 14 December 2012
10.1126/science.1230492

Stress State in the Largest Displacement Area of the 2011 Tohoku-Oki Earthquake

Weiren Lin,[1,2,3]* Marianne Conin,[4]† J. Casey Moore,[5] Frederick M. Chester,[6] Yasuyuki Nakamura,[7] James J. Mori,[8] Louise Anderson,[9] Emily E. Brodsky,[5] Nobuhisa Eguchi,[10] Expedition 343 Scientists‡

The 2011 moment magnitude 9.0 Tohoku-Oki earthquake produced a maximum coseismic slip of more than 50 meters near the Japan trench, which could result in a completely reduced stress state in the region. We tested this hypothesis by determining the in situ stress state of the frontal prism from boreholes drilled by the Integrated Ocean Drilling Program approximately 1 year after the earthquake and by inferring the pre-earthquake stress state. On the basis of the horizontal stress orientations and magnitudes estimated from borehole breakouts and the increase in coseismic displacement during propagation of the rupture to the trench axis, in situ horizontal stress decreased during the earthquake. The stress change suggests an active slip of the frontal plate interface, which is consistent with coseismic fault weakening and a nearly total stress drop.

The huge tsunami associated with the 2011 Tohoku-Oki earthquake [moment magnitude (M_w) 9.0] was caused by the very large coseismic fault displacement of the shallow portion of the subduction zone near the Japan trench (*1*–*5*). Besides the unprecedented large coseismic slip of >50 m, the other surprising feature of the earthquake is that the large slip on the frontal plate interface reached the sea floor at the trench axis (*6*). The state of stress and frictional behavior of the frontal plate interface is important for controlling coseismic displacement. Indirect analyses on stress state change and/or stress drop associated with the 2011 Tohoku-Oki earthquake have been carried out from remotely sensed observations (*7*–*12*).

To investigate the stress change associated with the 2011 Tohoku-Oki earthquake, we analyzed geophysical logs collected by the Integrated

[1]Kochi Institute for Core Sample Research, Japan Agency for Marine-Earth Science and Technology (JAMSTEC), Nankoku, Japan. [2]Geology Course, Graduate School of Arts and Sciences, Kochi University, Kochi, Japan. [3]Key Laboratory of Tectonics and Petroleum Resources of Ministry of Education, China University of Geosciences, Wuhan, China. [4]Centre Européen de Recherche et d'Enseignement des Géosciences de l'Environnement (CEREGE), Europôle Méditerranéen de l'Arbois, Aix en Provence, France. [5]Earth and Planetary Sciences Department, University of California, Santa Cruz, CA, USA. [6]Center for Tectonophysics, Department of Geology and Geophysics, Texas A&M University, College Station, TX, USA. [7]Institute for Research on Earth Evolution, JAMSTEC, Yokohama, Japan. [8]Disaster Prevention Research Institute, Kyoto University, Uji, Japan. [9]Department of Geology, University of Leicester, Leicester, UK. [10]Center for Deep Earth Exploration, JAMSTEC, Yokohama, Japan.

*To whom correspondence should be addressed. E-mail: lin@jamstec.go.jp
†Present address: EA4098 LaRGE, Université des Antilles et de la Guyane, Pointe-à-Pitre, France.
‡All authors with their affiliations appear at the end of this paper.

Downloaded from www.sciencemag.org on February 9, 2013

www.sciencemag.org/cgi/content/full/339/6120/684/DC1

Supplementary Materials for

Time Scales of Critical Events Around the Cretaceous-Paleogene Boundary

Paul R. Renne,* Alan L. Deino, Frederik J. Hilgen, Klaudia F. Kuiper, Darren F. Mark, William S. Mitchell III, Leah E. Morgan, Roland Mundil, Jan Smit

*To whom correspondence should be addressed. E-mail: prenne@bgc.org

Published 8 February 2013, *Science* **339**, 684 (2013)
DOI: 10.1126/science.1230492

This PDF file includes:

Other Supplementary Material for this manuscript includes the following:
(available at www.sciencemag.org/cgi/content/full/339/6120/684/DC1)

Data tables S1 to S4 (Microsoft Excel)

Materials and Methods

Sampling

Samples were collected by authors Renne and Deino in October, 2010, and by Renne, Mitchell and Mundil in September, 2011. Stratigraphic nomenclature follows Swisher *et al*. (*15*). The IrZ coal bentonite was sampled at two closely-spaced localities in the Hauso Flats (Iridium Hill) area: HF-1PR was sampled at 47°31.732' N latitude, 107°12.513'W longitude; HF-1AD and HF11-1 were sampled at 47°31.593' N latitude, 107°12.465' W longitude. The Z-coal bentonites (HC-1AD and HC-2PR) were sampled on the road to Hell Creek State Park at 47°31.593' N latitude, 106°56.397' W longitude. The HFZ coal bentonite (HF-3AD and HF-3PR) was collected near Hauso Flats at 47°31.502' N latitude, 107°11.987 W longitude. Coordinates are referenced to WGS84.

The IrZ coal in the sampling vicinity is about 10 cm thick, and is the stratigraphically lowest coal in the Hauso Flats area. The bentonite sampled is 2-4 mm thick, pinkish beige colored bed approximately 2 cm below the top of the coal and about 4 cm above the horizon containing impact signals (*14*).

The Z coal in the Hell Creek area is about 1.2 m thick and contains at least two distinct bentonites. The units sampled here were HC-1AD, the upper bentonite (hereinafter referred to as Z_1), and HC-2PR, the lower of these (hereinafter referred to as Z_2), about 80 cm below the top of the coal. The Z_1 bentonite (sample HC-1AD) is the most prominent of the two at this locality, is ~ 5 cm thick and contains conspicuous biotite. The Z_2 bentonite (sample HC-2PR) is about 2 cm thick, pinkish in color, and conspicuously crystal rich with sanidine but devoid of biotite. We suspect that most previous workers (*15*, *16*) reporting data from the Z coal in this vicinity sampled the thicker and more conspicuous upper bentonite corresponding to Z_1 (sample HC-1AD). Swisher *et al*. (*15*) appear to have sampled the same tuff (their sample 90CS-L1) as our Z_2 at this exact locality.

The HFZ coal occurs approximately 18 m stratigraphically above the IrZ coal in the Hauso Flats area, where it is ~2m thick. A ~1 cm thick bentonite occurs about 20 cm above the base of the coal, and contains visible pseudomorphs of glass shards, and feldspar crystals; this unit was sampled as HF-3. This bentonite appears to be distinct from the one sampled by Swisher *et al*. (*15*), which was collected "…within the upper part…" of the coal.

The tektites analyzed in this study were collected by F. Maurrasse from the Beloc section in Haiti from a ca. 10 cm interval between levels f and g (see Fig. 1 of Maurrasse and Sen (*7*)), coincident with an iridium anomaly and shocked quartz (*7*).

Analytical methods

Feldspars were separated from approximately 5 kg of each sample after disaggregating, washing and sieving followed by magnetic and density separations and finally ultrasonic

cleaning in 5% hydrofluoric acid for 5 minutes. Feldspars from the following size fractions were hand-picked for analysis: HF-3AD (251-422 μm), HC-1AD (178-251 μm), HC-2PR(178-251 μm) HF-1PR (251-422 μm), HF-1AD (178-251 μm), and HF11-1 (178-251 μm). Zircons were hand-picked from the dense portion of the <178 μm size fraction, preferentially selecting clear, euhedral, acicular crystals without visible cores. The Beloc tektites (sample HA91-13) were selected from the same sample analyzed by Swisher *et al*. (*12*). The tektites were prepared by ultrasonic cleaning in 5% hydrofluoric acid for 3 minutes to remove rinds of secondary clay minerals.

$^{40}Ar/^{39}Ar$ analyses were conducted at the Berkeley Geochronology Center (BGC) and the NERC Argon Isotope Facility, Scottish Universities Environmental Research Centre (SUERC). Samples analyzed at SUERC were run and reported blindly, without knowledge of the BGC results. U-Pb analyses were performed at BGC. The tektites and the Z_2 bentonite (HC-2PR) sanidine were irradiated together and analyzed at BGC. The two samples of the IrZ bentonite sanidines were irradiated in two disks in a single irradiation and an aliquot of sanidine and one of the bracketing standards from one disk (irradiation 400PR) were analyzed at SUERC. The second disk containing IrZ bentonite (HF-1AD) sanidines also contained the Z_1 (HC-1AD) and HFZ (HF-3AD) sanidine. Samples were irradiated in 50-hour irradiations in the CLICIT facility of the OSTR reactor. The irradiation scheme for each sample is depicted in Figure S3.

For the tektites (sample MA91-13) and Z-coal sanidines (sample HC-2PR) the three bracketing standard positions were used to monitor the neutron fluence. The weighted average $^{40}Ar^*/^{39}Ar_K$ was calculated for each well, and the arithmetic mean and standard deviation of these three values was used to characterize the neutron fluence for the unknowns. For the HF-1PR samples analyzed at BGC, an analogous approach was used with the four bracketing standards. For the HF-1PR samples analyzed at SUERC, the weighted mean of standards from one (BGC lab ID# 36501) of the four positions in irradiation 400PR was used. This was deemed sufficient as the BGC analyses revealed no significant variation between the four positions. For samples HF-1AD, HC-1AD, and HF-3, irradiated in the same disk (Figure S3) the $^{40}Ar^*/^{39}Ar_K$ of the standards at the positions of interest was determined by fitting a plane to the weighted mean values of standards from the four positions spanning the disk.

Samples were analyzed in several batches; backgrounds and mass discrimination measurements (via automated analysis of multiple air pipettes) specific to each batch are summarized in Table S1. Backgrounds subtracted from ion beam measurements were arithmetic averages and standard deviations. Mass discrimination was computed based on a power law relationship (*42*) using the isotopic composition of atmospheric Ar reported by (*43*). Corrections for radioactive decay of ^{39}Ar and ^{37}Ar were made using the decay constants reported by (*44*) and (*45*) respectively. Ingrowth of ^{36}Ar from decay of ^{36}Cl was corrected using the $^{36}Cl/^{38}Cl$ production ratio and methods of (*46*) and was determined to be negligible. Argon isotope data corrected for backgrounds, mass discrimination, and radioactive decay and ingrowth are given in Table S2.

Ages were computed from the blank-, discrimination- and decay-corrected Ar isotope data after correction for interfering isotopes based on the following production ratios, determined from fluorite and Fe-doped $KAlSiO_4$ glass irradiated along with the tektites and HC-2PR sanidine: $(^{36}Ar/^{37}Ar)_{Ca} = (2.650 \pm 0.022) \times 10^{-4}$; $(^{38}Ar/^{37}Ar)_{Ca} = (1.96 \pm 0.08) \times 10^{-5}$; $(^{39}Ar/^{37}Ar)_{Ca} = (6.95 \pm 0.09) \times 10^{-4}$; $(^{40}Ar/^{39}Ar)_{K} = (7.3 \pm 0.9) \times 10^{-4}$; $(^{38}Ar/^{39}Ar)_{K} = (1.215 \pm 0.003) \times 10^{-2}$; $(^{37}Ar/^{39}Ar)_{K} = (2.24 \pm 0.16) \times 10^{-4}$. Ages and their uncertainties are based on the methods of (*47*) and the calibration of (*17*) except where noted. Some of the authors (KFK and FJH) prefer the calibration of (*19*), which yields slightly younger ages in this time range, as discussed below. Age uncertainties shown in Table S2 include only analytical uncertainties.

For some of the age comparisons made herein, contributions from sources of systematic uncertainty (i.e., uncertainties in $^{40}Ar/^{40}K$ of the standard and ^{40}K decay constants) are neglected and only analytical uncertainties in isotope measurements of samples and standards are included. These uncertainties are referred to herein as "analytical uncertainties". For the purposes of this study analytical uncertainties include contributions from uncertainties in the interference corrections because these interference corrections have variable effects due to the variable chemistry of the samples considered. Where not otherwise distinguished, uncertainties are stated as X ±Y/Z, where Y is the analytical uncertainty as defined above, and Z is the full uncertainty considering both analytical and systematic sources of uncertainty.

Age computation uses the weighted (by inverse variance) mean of $^{40}Ar^*/^{39}Ar_K$ values for the sample and standard, combined as *R*-values and computed using the method of (*47*). Outliers in both single-crystal samples and standards were discriminated using a 3σ filter applied iteratively until all samples counted are within 3 standard deviations of the weighted mean ± one standard error. This procedure mainly screened older crystals that are logically interpreted as xenocrysts.

Zircons were annealed 60 h at 850 °C, and chemically abraded with hydrofluoric acid at 220 °C for 12 h (Mattinson, 2005). Individual zircons were dissolved for 1 week using the vapor transfer technique with hydrofluoric acid at 220 °C after addition of a ^{205}Pb-^{233}U-^{235}U spike. After dissolution, 15 µl of 3 *M* hydrochloric acid and 15 µl of 0.03 *M* H_3PO_4 were added to each sample, dried and loaded on zone-refined rhenium filaments with 4 µL silica gel solution (*48*) and evaporated to dryness.

Measurements were performed on a VG Sector 54 thermal ionization mass spectrometer using a single Daly detector in peak-jumping (dynamic) mode. Uranium was measured as UO_2, and corrected for oxygen isotope interferences. Mass fractionation corrections for Pb were made using repeated analysis of NBS-981 (see Table S4); U mass fractionation corrections were made using $^{233}U/^{235}U$ of the double spike.

BGC Results

The samples were analyzed by incremental heating or total fusion with CO_2 lasers on two different extraction systems mated to MAP 215 mass spectrometers (MAP1 and MAP3).

MAP1 is a 215C and MAP3 is a 215-50. Both have Nier-type ion sources and analog electron multiplier detectors. Mass spectrometry utilized peak-hopping by magnetic field switching on a single detector in 10-15 cycles.

Single crystal laser fusion $^{40}Ar/^{39}Ar$ results

44 feldspar crystals from sample HF-3AD of the HFZ coal bentonite were analyzed individually by total fusion followed by argon isotope analysis with the MAP3 mass spectrometer. All but one of the crystals (a plagioclase) analyzed proved to be alkali feldspars on the basis of K/Ca ratios. The plagioclase is an obvious xenocryst at 75.98 ± 2.03/2.03 Ma; this was excluded to yield a weighted mean age of 65.990 ± 0.032/0.053 Ma for the remaining 43 sanidines.

71 feldspar crystals from sample HC-1AD of the Z_1 coal bentonite were analyzed individually by total fusion followed by argon isotope analysis with the MAP3 mass spectrometer. All of the crystals analyzed proved to be alkali feldspars on the basis of K/Ca ratios. Excluding one outlier at 67.04 ± 0.29/0.30 Ma, the remaining 70 crystals yielded a unimodal age distribution with a weighted mean age of 66.003 ± 0.033/0.053 Ma.

86 feldspar crystals from sample HC-2PR of the Z_2 coal bentonite were analyzed individually by total fusion followed by argon isotope analysis with the MAP3 mass spectrometer. 70 of these proved to be sanidine, and the remainder plagioclase, on the basis of K/Ca ratios. Ages for the plagioclase crystals are imprecise due to their low K contents, but are indistinguishable from the sanidine results. Because the plagioclase data contribute negligibly to the result, they were excluded from further consideration. The age-distribution of sanidines (Figure 2) is unimodal and reveals no statistical outliers suggestive of xenocrysts. The sanidine crystals yielded a weighted mean age of 66.023 ± 0.053/0.067 Ma.

98 feldspar crystals from sample HF-1PR of the IrZ-coal bentonite were analyzed individually by total fusion followed by argon isotope analysis with the MAP1 mass spectrometer. All of the crystals analyzed proved to be alkali feldspars on the basis of K/Ca ratios. Neglecting one obvious xenocryst at 76.85 ± 0.22/0.28 Ma, the remaining 97 crystals yielded a unimodal age distribution with a weighted mean age of 66.039 ± 0.019/0.046 Ma.

86 feldspar crystals from sample HF-1AD of the IrZ-coal bentonite were analyzed individually by total fusion followed by argon isotope analysis with the MAP1 mass spectrometer. All of the crystals analyzed proved to be alkali feldspars on the basis of K/Ca ratios. Several crystals yielded anomalous ages as old as 81.35 ± 0.16/0.17 Ma and are unambiguously xenocrysts. The 3σ filter rejected 6 analyses from the old end of the distribution. Three of these grade essentially continuously into the rest of the distribution and we note that their exclusion is somewhat arbitrary. The remaining 80 grains yield a weighted mean age of 66.058 ± 0.030/0.052 Ma.

101 feldspar crystals from sample HF11-1 of the IrZ-coal bentonite were analyzed individually by total fusion followed by argon isotope analysis with the MAP1 mass spectrometer. All of the crystals analyzed proved to be alkali feldspars on the basis of K/Ca ratios. No outliers were detected. All 101 grains yielded a weighted mean age of 66.030 ± 0.040/0.058 Ma.

Incremental heating $^{40}Ar/^{39}Ar$ results

Incremental heating analysis was conducted on 14 tektites using both the MAP1 and the MAP3 mass spectrometers. Degassing of the tektites was conducted mainly using a defocused laser beam, but 3 exceptionally large tektites (in Run 3) were heated up to 40W using an integrator lens, then with a defocused beam for final degassing. These latter steps unintentionally released large fractions of the gas. The age spectra for 13/14 tektites are 100% concordant (plateaus comprising 100% of the ^{39}Ar released) and one comprises 99.5% of the ^{39}Ar released, consistent with previous experience. Ca/K ratios show some variation between steps in a given tektite, and integrated values range from 2.4 to 4.6 consistent with previous results from $^{40}Ar/^{39}Ar$ dating (*12*, *13*) as well as electron microprobe (*6*) studies. Plateau ages neglecting systematic errors range from 66.024 ± 0.091 to 66.095 ± 0.117 Ma considering analytical errors only, and are mutually indistinguishable as shown in Figure S4. The weighted mean of the 14 plateau ages is 66.038 ± 0.031/0.052 Ma.

Single crystal age distributions for the Z_2- and IrZ-coal bentonites validate collective analysis of multigrained aliquots by incremental heating. Accordingly, multigrain aliquots of feldspar were analyzed by incremental heating using an integrator lens to distribute beam power, with argon isotopes measured on MAP1. Two aliquots of ~15 crystals each of the Z_2-coal bentonite were analyzed in 32 and 26 steps up to 40W, and 5 aliquots of the IrZ coal bentonite were analyzed in 22-39 steps each up to 35W. The age spectra (Figure 2) for all aliquots are 100% concordant and yield plateau ages of 66.009 ± 0.032 and 66.028 ± 0.031 for the Z_2-coal bentonite, and range from 66.024 ± 0.030 to 66.085 ± 0.030 Ma for the IrZ-coal bentonite, considering analytical errors only. The pooled plateau ages are 66.019 ± 0.022/0.048 and 66.045 ± 0.017/0.045 Ma for the Z_2 and IrZ coal bentonites, respectively.

U-Pb results

17 zircons from the HFZ-coal bentonite (HF-3PR) were analyzed by CA-ID-TIMS (*49*, *50*). Three zircons yielded a $^{206}Pb/^{238}U$ age of >73 Ma, and were excluded from further analysis because of the significant inherited Pb component. Another zircon was reversely discordant, suggesting incomplete dissolution, and was excluded from analysis. The remaining 15 zircons yielded a weighted mean age of 65.988 ± 0.074 Ma. Analytical precision for $^{206}Pb/^{238}U$ on individual zircon analyses is limited to 0.1% due to low concentrations of radiogenic Pb resulting from small sample size (typically < 1 microgram per chemically abraded zircon). Analytical protocols follow those described by Mundil *et al*. (*49*). Interlaboratory calibration of the tracers used has been discussed elsewhere (*49*, *51*).

SUERC Results

The samples were analyzed by total fusion with a CO_2 laser and measurements made using a MAP 215-50 (MAP2) noble gas mass spectrometer. The mass spectrometer is equipped with a Nier-type ion source and analogue electron multiplier (Balzers SEV217). Mass spectrometry utilized peak-hopping by magnetic field switching on a single detector in 10 cycles.

40 feldspar crystals from the IrZ-coal bentonite (HF-1PR) were analyzed. All feldspar crystals proved to be alkali feldspars on the basis of K/Ca ratios. No data were rejected. The crystals yielded a normal age distribution with a weighted mean 66.041 ± 0.053/0.066 Ma.

Pooled $^{40}Ar/^{39}Ar$ ages

Pooled ages for the various bentonites are calculated from the weighted mean *R*-values corresponding to the single crystal total fusion and (where relevant) plateau ages. The *R*-values and their corresponding ages are shown in Table S3.

Previous results for the Beloc tektites were based on the Taylor Creek sanidine TCs) standard at 27.92 Ma (*13*) and FCs at 27.84 Ma (*12*). The data presented by Dalrymple *et al*. (*13*) included data previously reported by Izett *et al*. (*52*). Using the intercalibration between TCs and FCs and methods discussed by Renne *et al*. (*53*), these previous results can be represented as: $R_{FCs}^{Tektites} = 2.35941 \pm 0.00296$ (*12*) and $R_{FCs}^{Tektites} = 2.35734 \pm 0.00298$ (*13*). Our new data translate to a weighted mean value of $R_{FCs}^{Tektites} = 2.358674 \pm 0.001018$. The weighted mean of all three studies' results (Figure S5) is $R_{FCs}^{Tektites} = 2.358589 \pm 0.000916$, corresponding to an age of 66.038 ± 0.025/0.049 Ma according to the calibration of Renne *et al*. (*17*). The basis for the normalization is shown in Table S3.

Supplementary Text

High-precision radioisotopic dating of KPB-related events is based almost entirely on the $^{40}Ar/^{39}Ar$ method. Detailed comparison of $^{40}Ar/^{39}Ar$ ages, which were determined in several laboratories using different standards and various ages ascribed to these standards, requires normalizing these ages to a uniform basis. The most straightforward way to do this is to calculate values of a parameter termed *R* (*53*), which embodies the age of a sample relative to a standard. In the case of the KPB phenomena of interest here, all $^{40}Ar/^{39}Ar$ ages are either based on the Fish Canyon sanidine (FCs) standard or a standard (Taylor Creek sanidine; TCs) that has been intercalibrated with FCs (*53*). Relevant *R*-values for existing data, calculated using methods outlined by (*47*, *53*) are given in Table S3 and shown in Figure S1. The *R*-value for the Beloc tektites is the inverse-variance weighted average of results from (*13*) and (*12*).

The results indicate that the *R*-value of the IrZ bentonite with respect to the FCs standard as determined by Swisher *et al*. (*12*) exceeds that of the tektites and the Chicxulub melt

rocks by statistically significant margins of 0.0066 ± 0.0026 and 0.0066 ± 0.0024, respectively. Thus the IrZ bentonite, hence the KPB, appears resolvably older than either the tektites or the Chicxulub melt rocks based on existing data. Using the calibration of (*17*) and considering only analytical uncertainties, the corresponding age differences are 181 ± 71 ky and 183 ± 65 ky, respectively, a result that is independent of the calibration used. Thus the hypothesis that the Chicxulub impact was *not* synchronous with the KPB is supported by existing radiosotopic data, but in the opposite sense to that of Keller *et al*. (*54*) in that the Chicxulub structure and the associated tektites appear to have formed as much as 250 ky *after* the KPB at 68% confidence. Two important questions would follow from the diachrony either inferred (*54*) or implied by previous $^{40}Ar/^{39}Ar$ data: (1) since the KPB is clearly associated with impact signals in ubiquitous marine and terrestrial sections, where was the impact if not at Chicxulub? (2) were there no mass extinctions associated with the Chicxulub impact?

The possibility that the previous age reported (*15*) for the IrZ coal bentonite is incorrect was raised by Renne *et al*. (*47*), who noted an apparent inconsistency between results of their re-calibration of this age (66.236 ± 0.060 Ma) and the age (65.957 ± 0.040 Ma) for the KPB based on orbital tuning (*19*). The previous age (*15*) for the IrZ coal also bears scrutiny because it implies a sharp increase in sediment accumulation rate from 1.0 mm/ky in the bottom 2 m of the basal Paleogene to 6.5 mm/ky in the overlying 13 m of the Tullock Fm., increasing to 12.5 mm/ky in the uppermost 26 m of the Tullock Fm. (Figure S2). If valid, this could imply a rapid increase in erosion rates in the Tullock Fm. watershed within the first 200 ky of the Paleogene, possible evidence of climate change at the KPB. The anomalously low sediment accumulation rate in the basal 2 m of the Tullock Fm. suggests relatively slow erosion in the basal Tullock watershed, possibly indicating an arid climate in the aftermath of the KPB. An arid climate at this time would be inconsistent with pedological (*55*), stratigraphic and paleontological (*22*, *56–58*) evidence. On the other hand, it is possible that erosion rates and sediment fluxes were high during this interval, as suggested by numerous channel sand complexes in this stratigraphic interval (*22*, *57–59*), but that their net accumulation rate was low. Unfortunately there are no dated bentonites stratigraphically below the IrZ coal in the Hell Creek area, thus there is no basis to evaluate whether the previously reported age for the IrZ coal bentonite is anomalous in terms of implied sediment accumulation rates.

Comparison with orbital tuning chronologies and $^{40}Ar/^{39}Ar$ system calibration

Our absolute age (66.044 ± 0.045 Ma) for the terrestrial KPB as represented by the IrZ-coal bentonite is consistent with the preferred astronomical age (65.957 ± 0.040 Ma) of Kuiper *et al*. (*19*) for the KPB. The latter age is based on tuning the KPB in the marine Zumaia section of northern Spain (*60*) to the correlative 405-ky eccentricity minimum constrained by recalculating then published $^{40}Ar/^{39}Ar$ data for the KPB to an independently derived astronomically calibrated age of 28.201 ± 0.046 Ma for the FCs standard (*19*). Using this calibration (*19*), our new data for the IrZ-coal bentonite translates to 65.837 ± 0.061 Ma, providing slightly worse agreement with the astronomically tuned age for the KPB although still marginally indistinguishable within uncertainties at 95% confidence limit (Figure S6). Thus $^{40}Ar/^{39}Ar$ ages for the KPB based

on either (*19*) or (*17*) both support the preferred tuning of the Zumaia KTB proposed by (*19*), but not a 405 (or 810) ky younger tuning as proposed by Westerhold *et al*. (*21*, *61*). Application of a recently proposed astronomical FCs calibration (*62*) translates our new data for the IrZ-coal bentonite to 65.771 ± 0.060 Ma. This age is marginally consistent at 95% confidence with the tuned age of 65.957 Ma for the KPB, and inconsistent with the 405 ky younger tuning option (Figure S6).

Kuiper *et al*. (*19*) arrived at the astronomical KPB age of 65.957 Ma using the La2004 (*18*) solution for Earth's orbital motions. Two new sets of orbital solutions (La2010, (*63*); La2011, (*21*)) have become available in the interim, and these result in very similar ages for the KPB. Following the same tuning approach applied previously (*19*), i.e. the KPB is ~ 2.5 precession-related cycles below the oldest tuned 100-ky eccentricity minimum above KPB in combination with the average precession period of 21 ky at that time, the astronomical KPB age yields values ranging from 65.917 (La2010d, younger option) to 66.056 Ma (La2004, older option) as shown in Figure S7a-c. La2010a-c solutions are based on the short-term ephemeris INPOP08, while La2010d is based on the older INPOP06 ephemeris. However, the latter may in fact be more accurate as a consequence of problems encountered in INPOP08 (see (*21*)). La2010d yields a KPB age of 65.917 Ma, i.e. in better agreement with the FCs calibration of (*19*), although it cannot be excluded that the boundary should be tuned one ~100 ky cycle older when using this solution. Application of the almost identical La2011 solutions results in a KPB age in the same age range.

Use of the ~100 ky cycle for tuning should be avoided in principle as the new solutions are only reliable back to 50 Ma (La2010) or, potentially, 54 Ma (La2011), due to the chaotic behavior of the Solar System (*21*, *63*)). This limits the use of the ~100 ky (and 2.4 My) cycle further back in time, but the 405 ky cycle remains stable over much longer time intervals. We therefore also indicated ages of the correlative 405 ky eccentricity minimum in Figure S6 and S7a-c, which are very similar to the ages obtained previously (*19*).

At present, our preferred tuning of the KPB at Zumaia does not support discrimination between the $^{40}Ar/^{39}Ar$ calibrations of Renne *et al*. (*17*) and Kuiper *et al*. (*19*), because the astronomical age falls between the two options and is indistinguishable from either one. Our U/Pb age for the HFZ coal bentonite clearly supports the former calibration, but this is expected (and somewhat circular) due to the intrinsic role of U/Pb data in that calibration. However, some recently proposed $^{40}Ar/^{39}Ar$ calibrations, such as the radical one based on ice-volume models for the age of the Matuyama-Brunhes geomagnetic polarity reversal (*64*), are clearly inconsistent with our preferred tuning, suggesting that the KPB should be tuned one or even two 405 ky eccentricity minima younger. In fact, the latter has recently been suggested (*21*), but we consider this option improbable because the corresponding inferred age of 27.93 Ma (*64*), or 27.89 Ma (*21*) for the FCs standard is clearly at odds with the two other independent astronomical calibrations (*19*); (*62*)) and with the optimization approach (*17*). Moreover, Kuiper *et al*. (*19*) and Hilgen *et al*. (*65*) provided an alternative cyclostratigraphic interpretation with the lower Paleocene containing one extra 405 ky cycle, while a direct comparison between a radioisotopic and

astronomical age model for the Early Eocene revealed an abrupt discrepancy of ~500 ky around 50 Ma (*66*) that may point to another 405 ky cycle that has been overlooked in the astronomical age model of Westerhold *et al*. (*21*).

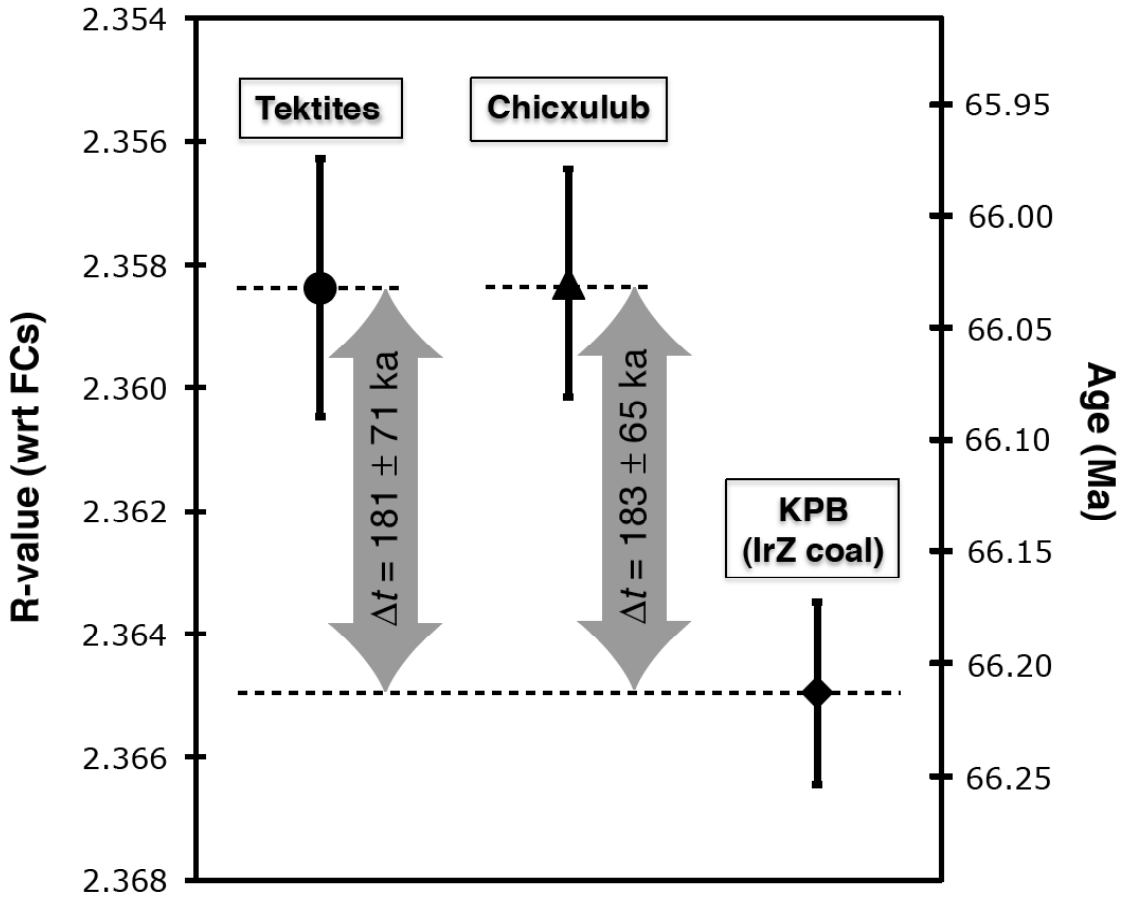

Fig. S1.
Existing $^{40}Ar/^{39}Ar$ data (*12*, *13*) show that the Haitian tektites were synchronous with the Chicxulub impact melt rocks, but that they may have been separated in time by as much as 79 ky. Existing $^{40}Ar/^{39}Ar$ data (*15*) indicate that the KPB predates the tektites and the Chicxulub impact event by 181 ± 71 and 183 ± 65 ky, respectively.

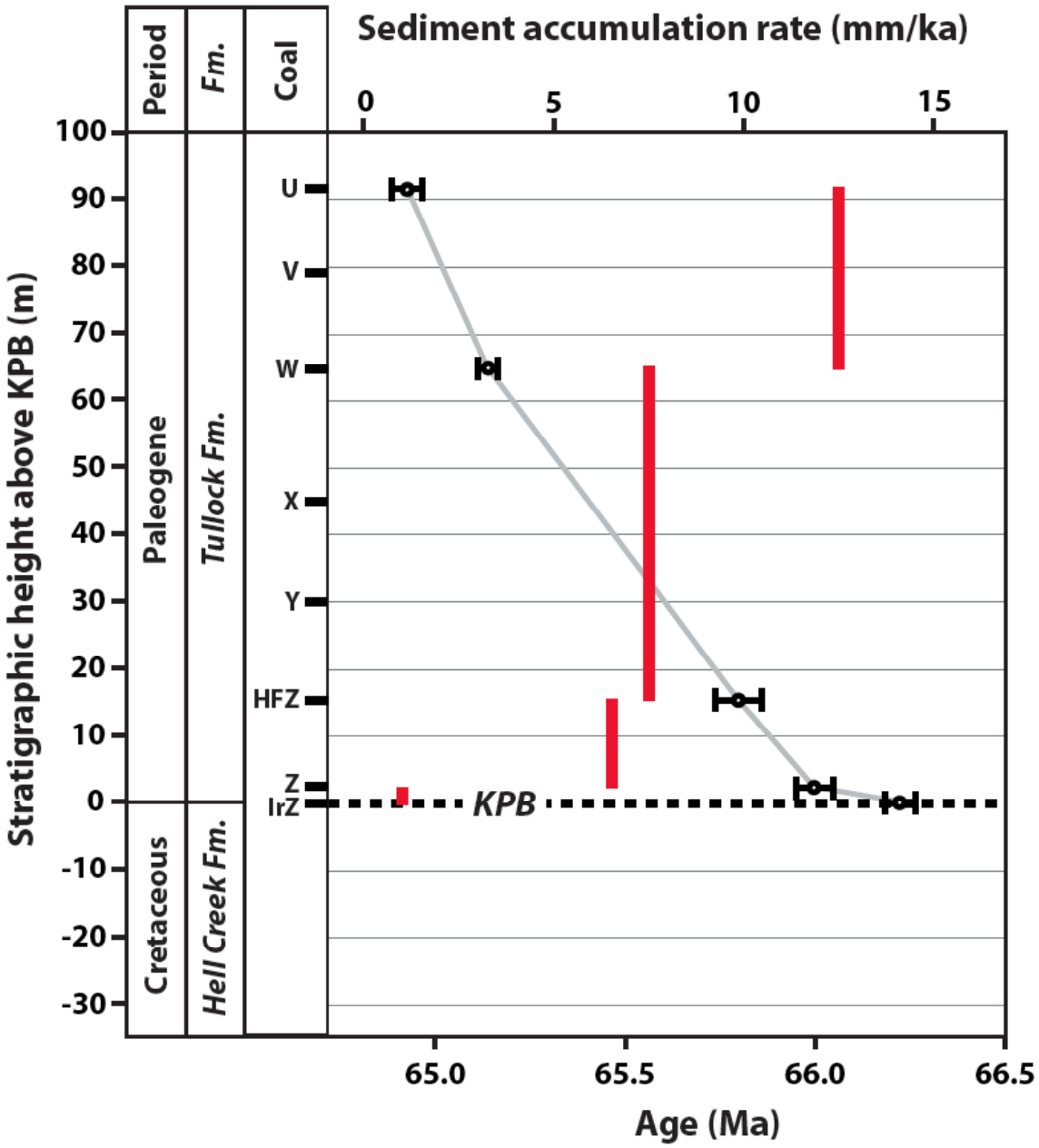

Fig. S2

Composite stratigraphy and sediment accumulation history for the basal Paleogene Tullock Formation indicated by previous $^{40}Ar/^{39}Ar$ dating (*15*). Samples reported here come from bentonites in the lowest three coal beds shown, labeled IrZ, Z, and HFZ. The previous data suggest an exceptionally low average accumulation rate for the lowermost 2 m of the section, increasing rapidly above the Z-coal. Accumulation rate for each interval between dated tuffs shown by red bars, with scale at top of plot.

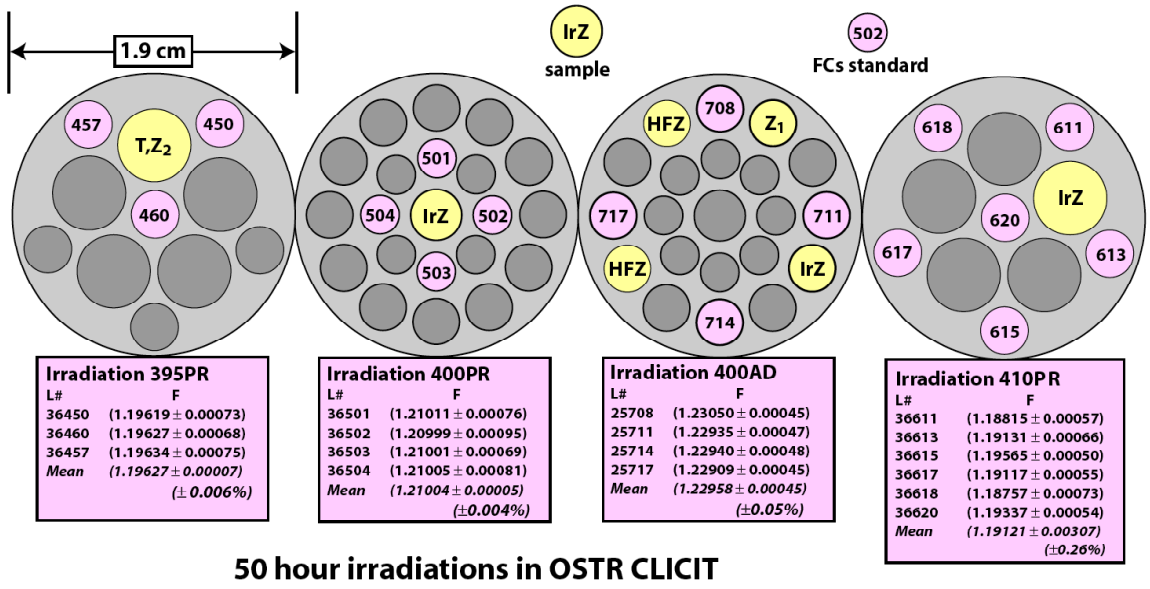

Fig. S3

Irradiation disc maps showing locations of relevant samples and standards, and values of F ($^{40}Ar^*/^{39}Ar_K$) for the standards. F-values shown for each L# are weighted mean values for all standard grains in that well, whereas mean values are the arithmetic mean and standard deviation of the individual well numbers. Mean F-value for Irradiations 400AD and 410PR are shown for comparison only; for these irradiations a planar fit was used to determine the F-value of the standard at each unknown position (shown in Table S2).

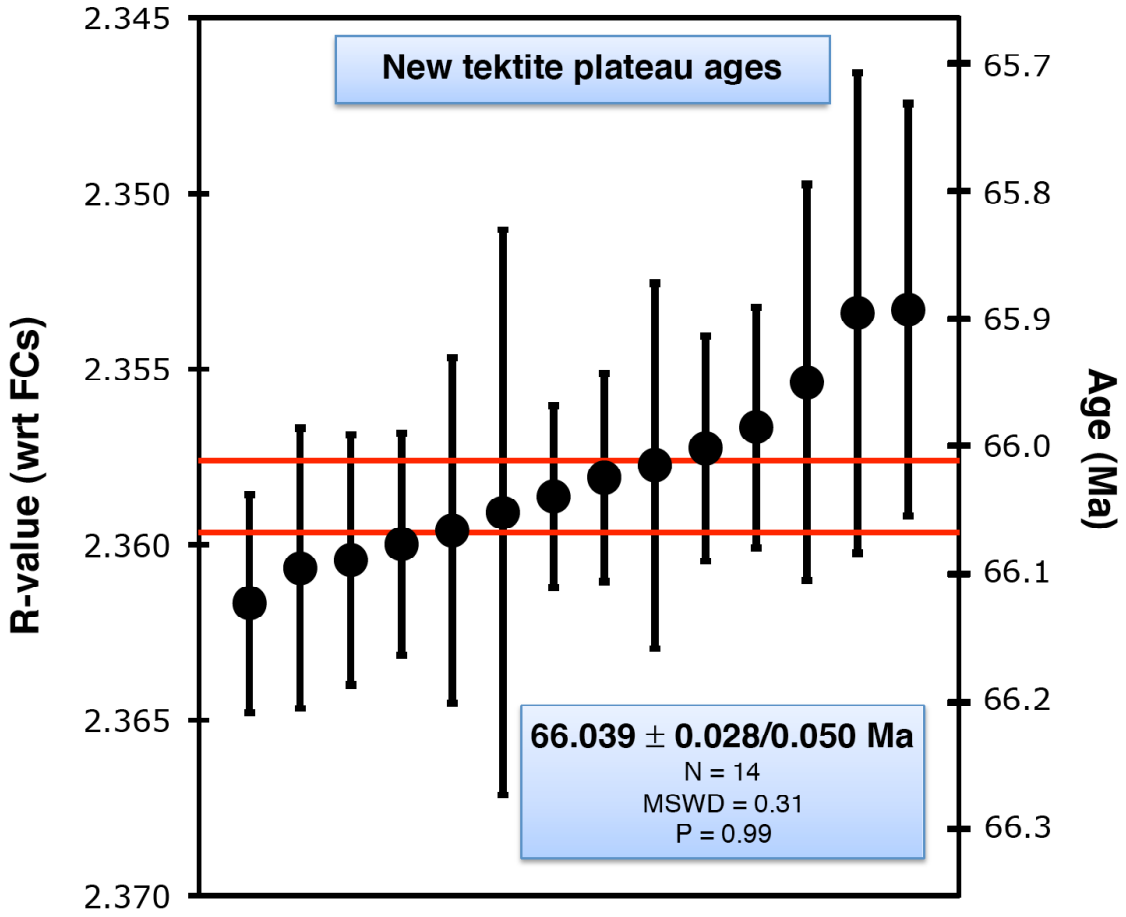

Fig. S4

Summary of plateau ages for new analyses of tektites. Ages are shown in rank order. Red lines delimit one standard error of the mean, excluding systematic uncertainties.

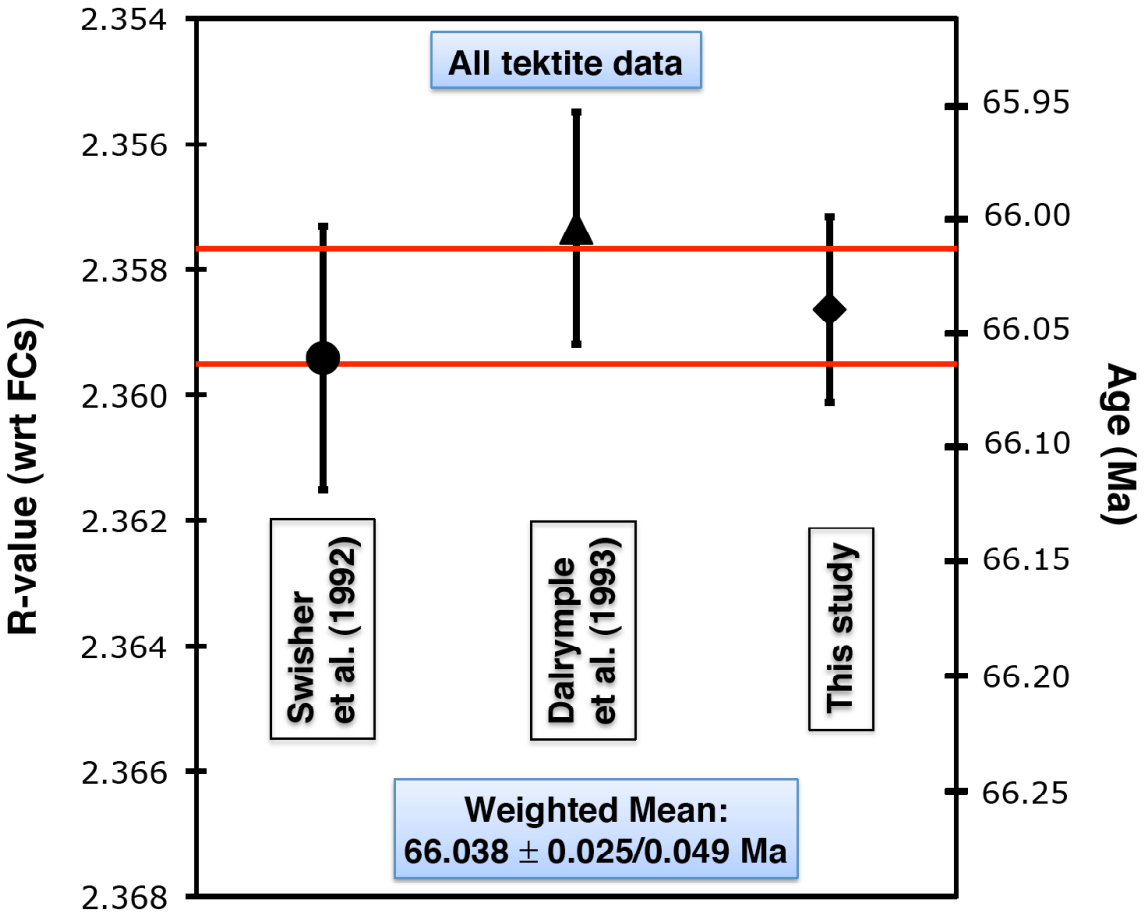

Fig. S5

Interlaboratory summary of tektite data from previous studies indicated and new data (This study). Red lines delimit one standard error of the mean, excluding systematic uncertainties.

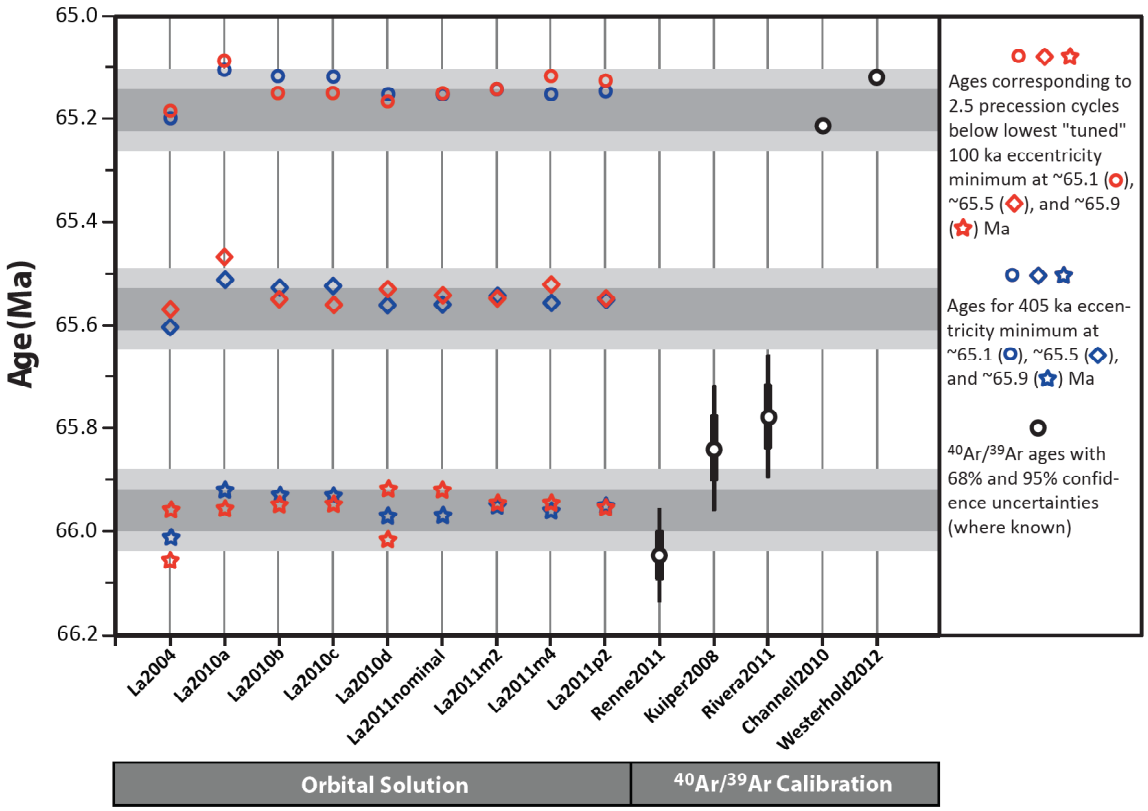

Fig. S6

Astronomical ages for the KPB based on tuning to recent orbital solutions (La2004: (*18*); La2010a-d: (*42*); La2011: (*21*)), using different tuning approaches and for three options that are one 405 ky eccentricity cycle apart, compared with $^{40}Ar/^{39}Ar$ ages of Ir-Z coal calculated for different calibrations. KPB ages shown for the three options are based on the identification and tuning of ~100 ky cycles with the boundary located 2.5 precession below the last 100 ky minimum (in red, dark green and dark blue) as in Kuiper *et al.* (2008). For a limited number of solutions, two options are presented which are 100 ky apart and considered equally likely in view of the cycle patterns in the lower 10m of the Zumaia section. As the 100 ky cycle is not reliable in the astronomical solutions (see text), we also provide the age of the 405 ky minimum (in blue) that approximates the KPB. Grey shaded area presents astronomically tuned KPB age based on Kuiper *et al.* (*19*) with 1 (dark grey: ±40 ky) and 2 (light grey) sigma errors for tuning to the 3 different 405 ky eccentricity minima options.

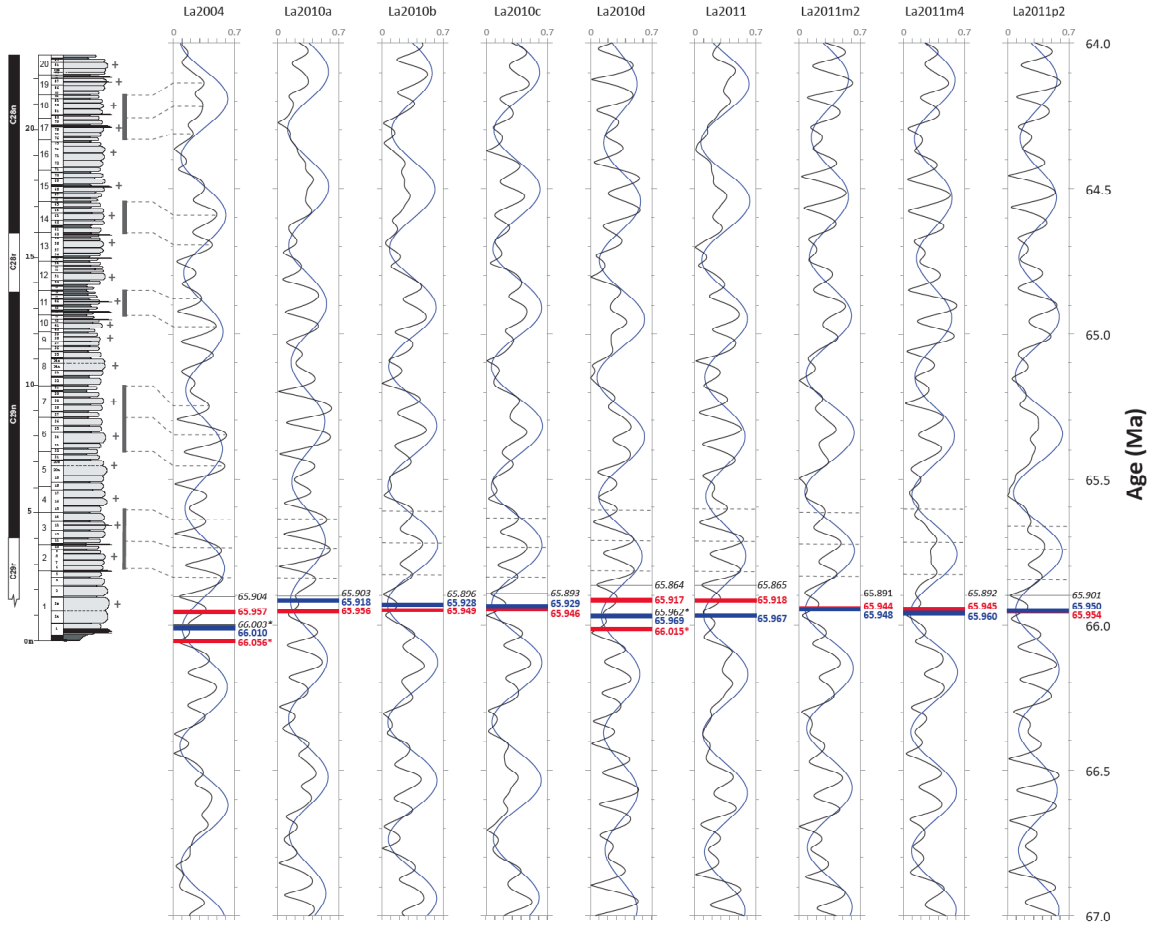

Fig. S7(a)

Tuning of the KPB in the Zumaia section to recent astronomical solutions (La2004: (*18*); La2010a-d: (*42*); La2011: (*21*)), for each of three (a-c) choices of 405 ky eccentricity cycles. In each case, the results of two different approaches are shown. KPB ages are shown based on the identification and tuning of ~100 ky cycles with the boundary located 2.5 precession below the last 100 ky minimum (in red) as in Kuiper *et al*. (*19*). This tuning is constrained by the expression of three distinct 100 ky maxima in the interval that corresponds with the first 405 ky maximum above the KPB at Zumaia. For a limited number of solutions, two options are presented which are 100 ky apart and considered equally likely in view of the cycle patterns in the lower 10m of the Zumaia section (older option marked with asterisk). As the 100 ky cycle is not reliable in the astronomical solutions (see text), we also provide the age of the 405 ky minimum (in blue) that approximates the KPB.

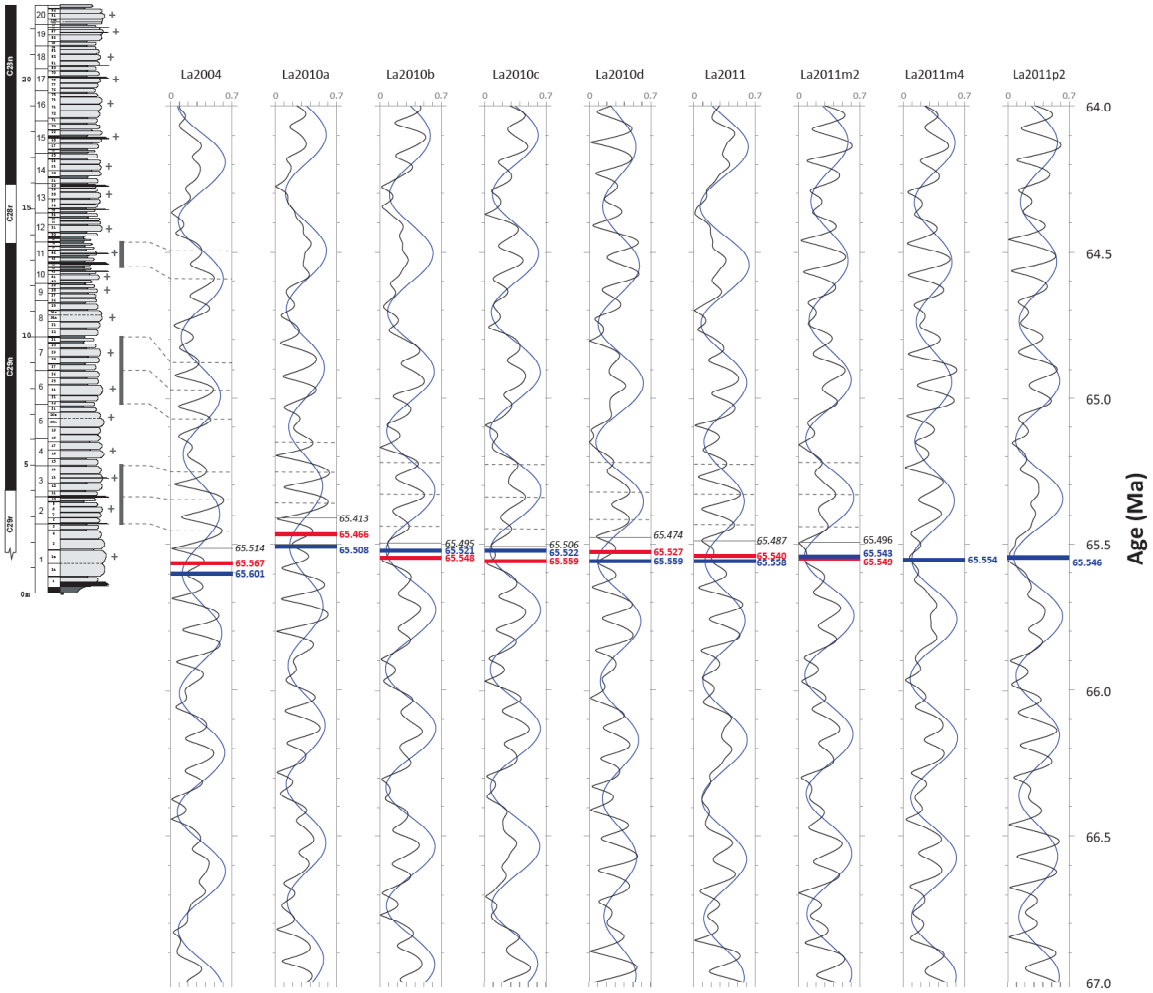

Fig. S7(b)

Caption as in Fig. S7(a) above.

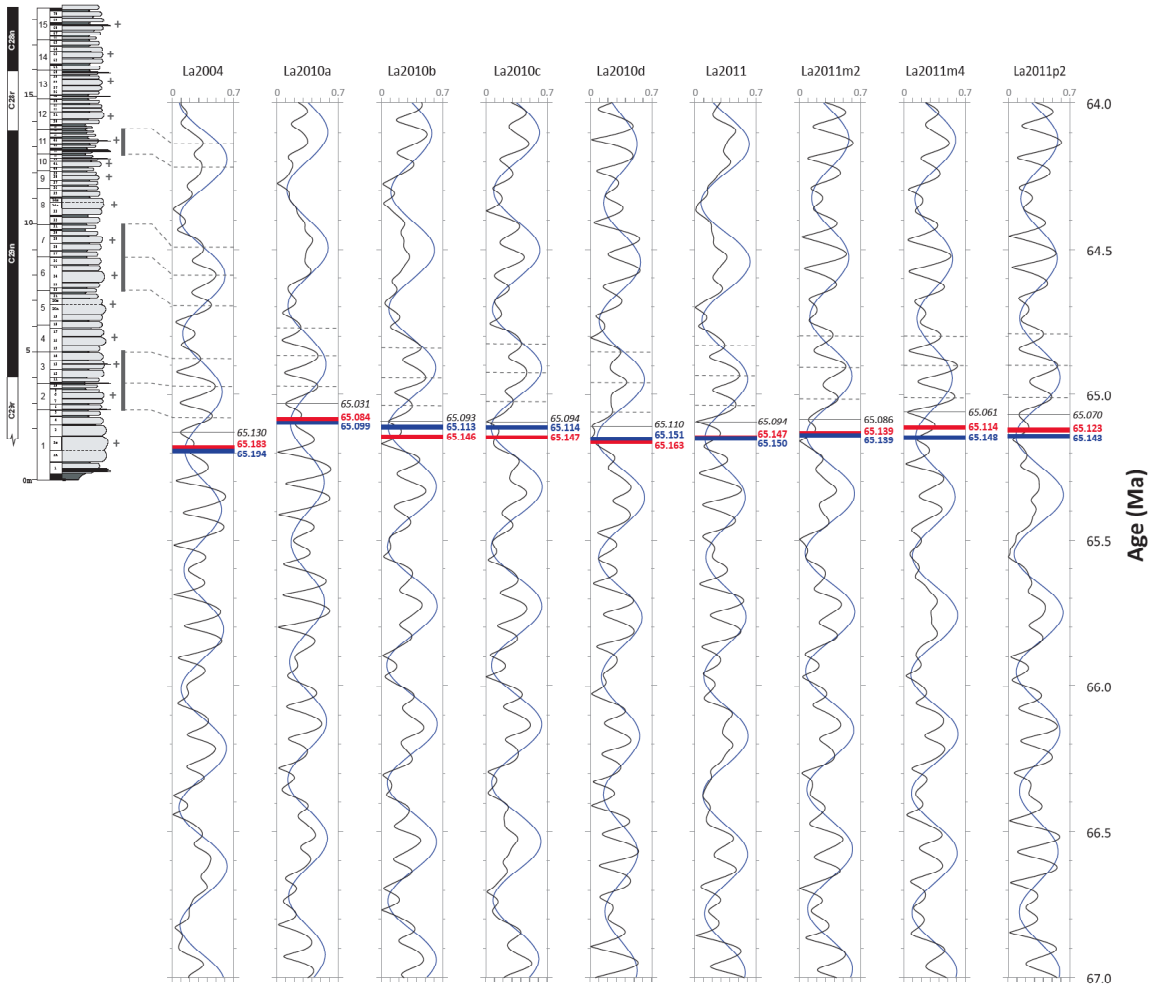

Fig. S7(c)
Caption as in Fig. S7(a) above.

Data table S1 (separate file)

Summary of run parameters for $^{40}Ar/^{39}Ar$ analyses (mass discrimination, backgrounds) specific to each run as identified in Table S2.

Data table S2 (separate file)

$^{40}Ar/^{39}Ar$ analytical data.

Data table S3 (separate file)

Summary of new and previous $^{40}Ar/^{39}Ar$ data showing the basis for normalization to a uniform calibration.

Data table S4 (separate file)

U-Pb analytical data. Pb blank composition for analyses using the BW ^{205}Pb-^{233}U-^{235}U spike is $^{206}Pb/^{204}Pb = 18.55 \pm 0.63$, $^{207}Pb/^{204}Pb = 15.50 \pm 0.55$, $^{208}Pb/^{204}Pb = 38.07 \pm 1.56$, and a $^{206}Pb/^{204}Pb$-$^{207}Pb/^{204}Pb$ correlation of +0.9. For analyses using the BDS ^{205}Pb-^{233}U-^{235}U spike, the blank composition is $^{206}Pb/^{204}Pb = 18.47 \pm 0.34$, $^{207}Pb/^{204}Pb = 15.63 \pm 0.21$, $^{208}Pb/^{204}Pb = 38.05 \pm 1.40$ (uncertainties here are all 2σ of population), and a $^{206}Pb/^{204}Pb$-$^{207}Pb/^{204}Pb$ correlation of +0.78. Present day Th/U ratio is calculated from radiogenic $^{208}Pb/^{206}Pb$ and age. Isotopic ratios are corrected for tracer contribution and mass fractionation (0.15 ± 0.09 %/amu). Ratios of radiogenic Pb versus U are corrected for mass fractionation, tracer contribution and common Pb contribution. ρ is correlation coefficient of radiogenic $^{207}Pb/^{235}U$ versus $^{206}Pb/^{238}U$. Uncertainties of individual ratios and ages are given at the 2σ level and do not include decay constant errors. Ratios involving ^{206}Pb are corrected for initial disequilibrium in $^{230}Th/^{238}U$ adopting Th/U=4 for the crystallization environment, resulting in a correction of ca. 80 ky.

References and Notes

1. P. Schulte *et al*., The Chicxulub asteroid impact and mass extinction at the Cretaceous-Paleogene boundary. *Science* **327**, 1214 (2010). doi:10.1126/science.1177265 Medline

2. J. D. Archibald *et al*., Cretaceous extinctions: Multiple causes. *Science* **328**, 973, author reply 975 (2010). doi:10.1126/science.328.5981.973-a Medline

3. V. Courtillot, F. Fluteau, Cretaceous extinctions: The volcanic hypothesis. *Science* **328**, 973, author reply 975 (2010). doi:10.1126/science.328.5981.973-b Medline

4. G. Keller *et al*., Cretaceous extinctions: Evidence overlooked. *Science* **328**, 974, author reply 975 (2010). doi:10.1126/science.328.5981.974-a Medline

5. N. C. Arens, I. D. West, Press-pulse: A general theory of mass extinction? *Paleobiology* **34**, 456 (2008). doi:10.1666/07034.1

6. H. Sigurdsson *et al*., Geochemical constraints on source region of Cretaceous/Tertiary impact glasses. *Nature* **353**, 839 (1991). doi:10.1038/353839a0

7. F. J. Maurrasse, G. Sen, Impacts, tsunamis, and the Haitian Cretaceous-Tertiary boundary layer. *Science* **252**, 1690 (1991). doi:10.1126/science.252.5013.1690 Medline

8. A. R. Hildebrand *et al*., Chicxulub Crater: A possible Cretaceous/Tertiary boundary impact crater on the Yucatán Peninsula, Mexico. *Geology* **19**, 867 (1991). doi:10.1130/0091-7613(1991)019<0867:CCAPCT>2.3.CO;2

9. Uncertainties here and throughout are stated at the 68% confidence level.

10. G. Keller *et al*., Chicxulub impact predates K–T boundary: New evidence from Brazos, Texas. *Earth Planet. Sci. Lett.* **255**, 339 (2007). doi:10.1016/j.epsl.2006.12.026

11. Uncertainties given as ±X/Y refer to values excluding (X) and including (Y) systematic sources as defined in the supplementary material.

12. C. C. Swisher III *et al*., Coeval $^{40}Ar/^{39}Ar$ Ages of 65.0 million years ago from Chicxulub Crater melt rock and Cretaceous-Tertiary boundary tektites. *Science* **257**, 954 (1992). doi:10.1126/science.257.5072.954 Medline

13. G. B. Dalrymple, G. A. Izett, L. W. Snee, J. D. Obradovich, *U.S. Geol. Surv. Bull.* **2065**, 1 (1993).

14. J. Smit, S. van der Kaars, Terminal cretaceous extinctions in the hell creek area, montana: Compatible with catastrophic extinction. *Science* **223**, 1177 (1984). doi:10.1126/science.223.4641.1177 Medline

15. C. C. Swisher III, L. Dingus, R. F. Butler, $^{40}Ar/^{39}Ar$ dating and magnetostratigraphic correlation of the terrestrial Cretaceous–Paleogene boundary and Puercan Mammal Age, Hell Creek–Tullock formations, eastern Montana. *Can. J. Earth Sci.* **30**, 1981 (1993). doi:10.1139/e93-174

16. H. Baadsgaard, J. F. Lerbekmo, I. McDougall, *Can. J. Earth Sci.* **25**, 1088 (1988).

17. P. R. Renne, G. Balco, K. R. Ludwig, R. Mundil, K. Min, Response to the comment by W. H. Schwarz *et al*. on "Joint determination of ^{40}K decay constants and ^{40}Ar∗/^{40}K for the Fish Canyon sanidine standard, and improved accuracy for ^{40}Ar/^{39}Ar geochronology" by P. R. Renne *et al*. (2010). *Geochim. Cosmochim. Acta* **75**, 5097 (2011). doi:10.1016/j.gca.2011.06.021

18. J. Laskar *et al*., A long-term numerical solution for the insolation quantities of the Earth. *Astron. Astrophys.* **428**, 261 (2004). doi:10.1051/0004-6361:20041335

19. K. F. Kuiper *et al*., Synchronizing rock clocks of Earth history. *Science* **320**, 500 (2008). doi:10.1126/science.1154339 Medline

20. D. Husson *et al*., Astronomical calibration of the Maastrichtian (Late Cretaceous). *Earth Planet. Sci. Lett.* **305**, 328 (2011). doi:10.1016/j.epsl.2011.03.008

21. T. Westerhold, U. Rohl, J. Laskar, Time scale controversy: Accurate orbital calibration of the early Paleogene. *Geochem. Geophys. Geosyst.* **13**, Q06015 (2012). doi:10.1029/2012GC004096

22. W. A. Clemens, in *The Hell Creek Formation and the Cretaceous-Tertiary Boundary in the Northern Great Plains: An Integrated Continental Record of the End of the Cretaceous,* J. H. Hartman, K. R. Johnson, D. J. Nichols, Eds. (Geological Society of America, Boulder, CO, 2002), vol. 361, pp. 217–245.

23. J. C. Avise, D. Walker, G. C. Johns, Speciation durations and Pleistocene effects on vertebrate phylogeography. *Proc. R. Soc. Lond. B Biol. Sci.* **265**, 1707 (1998). doi:10.1098/rspb.1998.0492

24. N. C. Arens, A. H. Jahren, Carbon isotope excursion in atmospheric CO_2 at the Cretaceous-Tertiary Boundary: Evidence from terrestrial sediments. *Palaios* **15**, 314 (2000). doi:10.1669/0883-1351(2000)015<0314:CIEIAC>2.0.CO;2

25. J. Smit, *Geol. Mijnb.* **69**, 187 (1990).

26. S. D'Hondt, Consequences of the Cretaceous/Paleogene mass extinction for marine ecosystems. *Annu. Rev. Ecol. Evol. Syst.* **36**, 295 (2005). doi:10.1146/annurev.ecolsys.35.021103.105715

27. L. Q. Li, G. Keller, Maastrichtian climate, productivity and faunal turnovers in planktic foraminifera in South Atlantic DSDP sites 525A and 21. *Mar. Micropaleontol.* **33**, 55 (1998). doi:10.1016/S0377-8398(97)00027-3

28. E. Barrera, S. M. Savin, in *Evolution of the Cretaceous Ocean-Climate System,* E. Barrera, C. C. Johnson, Eds. (Geological Society of America, Boulder, CO, 1999), vol. 332.

29. P. Wilf, K. R. Johnson, B. T. Huber, Correlated terrestrial and marine evidence for global climate changes before mass extinction at the Cretaceous-Paleogene boundary. *Proc. Natl. Acad. Sci. U.S.A.* **100**, 599 (2003). doi:10.1073/pnas.0234701100 Medline

30. G. P. Wilson, Mammalian faunal dynamics during the last 1.8 million years of the Cretaceous in Garfield County, Montana. *J. Mamm. Evol.* **12**, 53 (2005). doi:10.1007/s10914-005-6943-4

31. E. C. Murphy, J. W. Hoganson, K. R. Johnson, in *The Hell Creek Formation and the Cretaceous-Tertiary Boundary in the Northern Great Plains: An Integrated Continental Record of the End of the Cretaceous*, J. H. Hartman, K. R. Johnson, D. J. Nichols, Eds. (Geological Society of America, Boulder, CO, 2002), pp. 9–34.

32. K. G. Miller *et al*., The Phanerozoic record of global sea-level change. *Science* **310**, 1293 (2005). doi:10.1126/science.1116412 Medline

33. A. D. Barnosky *et al*., Approaching a state shift in Earth's biosphere. *Nature* **486**, 52 (2012). doi:10.1038/nature11018 Medline

34. M. Scheffer *et al*., Early-warning signals for critical transitions. *Nature* **461**, 53 (2009). doi:10.1038/nature08227 Medline

35. S. Self, The effects and consequences of very large explosive volcanic eruptions. *Philos. Trans. R. Soc. Lond. A* **364**, 2073 (2006). doi:10.1098/rsta.2006.1814

36. A. L. Chenet *et al*., Determination of rapid Deccan eruptions across the Cretaceous-Tertiary boundary using paleomagnetic secular variation: 2. Constraints from analysis of eight new sections and synthesis for a 3500-m-thick composite section. *J. Geophys. Res. Solid Earth* **114**, B06103 (2009). doi:10.1029/2008JB005644

37. G. Keller, Cretaceous climate, volcanism, impacts, and biotic effects. *Cretac. Res.* **29**, 754 (2008). doi:10.1016/j.cretres.2008.05.030

38. V. E. Courtillot, P. R. Renne, On the ages of flood basalt events. *C. R. Geosci.* **335**, 113 (2003). doi:10.1016/S1631-0713(03)00006-3

39. N. Robinson, G. Ravizza, R. Coccioni, B. Peucker-Ehrenbrink, R. Norris, A high-resolution marine $^{187}Os/^{188}Os$ record for the late Maastrichtian: Distinguishing the chemical fingerprints of Deccan volcanism and the KP impact event. *Earth Planet. Sci. Lett.* **281**, 159 (2009). doi:10.1016/j.epsl.2009.02.019

40. T. S. Tobin *et al.*, Extinction patterns, $\delta^{18}O$ trends, and magnetostratigraphy from a southern high-latitude Cretaceous–Paleogene section: Links with Deccan volcanism. *Palaeogeogr. Palaeoclimatol. Palaeoecol.* **350–352**, 180 (2012).

41. L. W. Alvarez, Experimental evidence that an asteroid impact led to the extinction of many species 65 million years ago. *Proc. Natl. Acad. Sci. U.S.A.* **80**, 627 (1983). doi:10.1073/pnas.80.2.627 Medline

42. P. R. Renne, W. S. Cassata, L. E. Morgan, The isotopic composition of atmospheric argon and $^{40}Ar/^{39}Ar$ geochronology: Time for a change? *Quat. Geochronol.* **4**, 288 (2009). doi:10.1016/j.quageo.2009.02.015

43. J. Y. Lee *et al*., A redetermination of the isotopic abundances of atmospheric Ar. *Geochim. Cosmochim. Acta* **70**, 4507 (2006). doi:10.1016/j.gca.2006.06.1563

44. R. W. Stoenner, O. A. Schaeffer, S. Katcoff, Half-Lives of Argon-37, Argon-39, and Argon-42. *Science* **148**, 1325 (1965). doi:10.1126/science.148.3675.1325 Medline

45. P. R. Renne, E. B. Norman, Determination of the half-life of ^{37}Ar by mass spectrometry. *Phys. Rev. C Nucl. Phys.* **63**, 047302 (2001). doi:10.1103/PhysRevC.63.047302

46. P. R. Renne, Z. D. Sharp, M. T. Heizler, Cl-derived argon isotope production in the CLICIT facility of OSTR reactor and the effects of the Cl-correction in ^{40}Ar/^{39}Ar geochronology. *Chem. Geol.* **255**, 463 (2008). doi:10.1016/j.chemgeo.2008.07.014

47. P. R. Renne, R. Mundil, G. Balco, K. W. Min, K. R. Ludwig, Joint determination of 40K decay constants and ^{40}Ar∗/^{40}K for the Fish Canyon sanidine standard, and improved accuracy for ^{40}Ar/^{39}Ar geochronology. *Geochim. Cosmochim. Acta* **74**, 5349 (2010). doi:10.1016/j.gca.2010.06.017

48. H. Gerstenberger, G. Haase, A highly effective emitter substance for mass spectrometric Pb isotope ratio determinations. *Chem. Geol.* **136**, 309 (1997). doi:10.1016/S0009-2541(96)00033-2

49. R. Mundil, K. R. Ludwig, I. Metcalfe, P. R. Renne, Age and timing of the Permian mass extinctions: U/Pb dating of closed-system zircons. *Science* **305**, 1760 (2004). doi:10.1126/science.1101012 Medline

50. J. M. Mattinson, Zircon U–Pb chemical abrasion ("CA-TIMS") method: Combined annealing and multi-step partial dissolution analysis for improved precision and accuracy of zircon ages. *Chem. Geol.* **220**, 47 (2005). doi:10.1016/j.chemgeo.2005.03.011

51. R. B. Irmis, R. Mundil, J. W. Martz, W. G. Parker, High-resolution U–Pb ages from the Upper Triassic Chinle Formation (New Mexico, USA) support a diachronous rise of dinosaurs. *Earth Planet. Sci. Lett.* **309**, 258 (2011). doi:10.1016/j.epsl.2011.07.015

52. G. A. Izett, G. B. Dalrymple, L. W. Snee, ^{40}Ar/^{39}Ar age of Cretaceous-Tertiary boundary tektites from Haiti. *Science* **252**, 1539 (1991). doi:10.1126/science.252.5012.1539 Medline

53. P. R. Renne *et al.*, Intercalibration of standards, absolute ages and uncertainties in ^{40}Ar/^{39}Ar dating. *Chem. Geol.* **145**, 117 (1998). doi:10.1016/S0009-2541(97)00159-9

54. G. Keller, W. Stinnesbeck, T. Adatte, D. Stuben, Multiple impacts across the Cretaceous–Tertiary boundary. *Earth Sci. Rev.* **62**, 327 (2003). doi:10.1016/S0012-8252(02)00162-9

55. G. J. Retallack, A pedotype approach to latest Cretaceous and earliest Tertiary paleosols in eastern Montana. *Geol. Soc. Am. Bull.* **106**, 1377 (1994). doi:10.1130/0016-7606(1994)106<1377:APATLC>2.3.CO;2

56. P. M. Sheehan, D. E. Fastovsky, Major extinctions of land-dwelling vertebrates at the Cretaceous-Tertiary boundary, eastern Montana. *Geology* **20**, 556 (1992). doi:10.1130/0091-7613(1992)020<0556:MEOLDV>2.3.CO;2

57. J. D. Archibald, *A Study of Mammalia and Geology Across the Cretaceous-Tertiary Boundary in Garfield County, Montana*, Univ. of California Publications in Geological Sciences (Univ of California Press, Berkeley, 1982), vol. 122.

58. D. L. Lofgren, *The Bug Creek Problem and the Cretaceous-Tertiary Transition at McGuire Creek, Montana*, Univ. of California Publications in Geological Sciences (Univ. of California Press, Berkeley, 1995), vol. 140.

59. D. E. Fastovsky, R. H. Dott Jr., Sedimentology, stratigraphy, and extinctions during the Cretaceous-Paleogene transition at Bug Creek, Montana. *Geology* **14**, 279 (1986). doi:10.1130/0091-7613(1986)14<279:SSAEDT>2.0.CO;2

60. J. Dinarés-Turell *et al*., Untangling the Palaeocene climatic rhythm: An astronomically calibrated Early Palaeocene magnetostratigraphy and biostratigraphy at Zumaia (Basque basin, northern Spain). *Earth Planet. Sci. Lett.* **216**, 483 (2003). doi:10.1016/S0012-821X(03)00557-0

61. T. Westerhold *et al*., Astronomical calibration of the Paleocene time. *Palaeogeogr. Palaeoclimatol. Palaeoecol.* **257**, 377 (2008). doi:10.1016/j.palaeo.2007.09.016

62. T. A. Rivera, M. Storey, C. Zeeden, F. J. Hilgen, K. Kuiper, A refined astronomically calibrated $^{40}Ar/^{39}Ar$ age for Fish Canyon sanidine. *Earth Planet. Sci. Lett.* **311**, 420 (2011). doi:10.1016/j.epsl.2011.09.017

63. J. Laskar, A. Fienga, M. Gastineau, H. Manche, La2010: A new orbital solution for the long-term motion of the Earth. *Astron. Astrophys.* **532**, A89 (2011). 10.1051/0004-6361/201116836

64. J. E. T. Channell, D. A. Hodell, B. S. Singer, C. Xuan, Reconciling astrochronological and $^{40}Ar/^{39}Ar$ ages for the Matuyama-Brunhes boundary and late Matuyama Chron. *Geochem. Geophys. Geosyst.* **11**, Q0AA12 (2010). doi:10.1029/2010GC003203

65. F. J. Hilgen, K. F. Kuiper, L. J. Lourens, Evaluation of the astronomical time scale for the Paleocene and earliest Eocene. *Earth Planet. Sci. Lett.* **300**, 139 (2010). doi:10.1016/j.epsl.2010.09.044

66. N. Vandenberghe, R. Speijer, F. J. Hilgen, in *The Geologic Time Scale 2012,* F. J. Gradstein, J. G. Ogg, M. D. Schmitz, G. Ogg, Eds. (Elsevier, Amsterdam, 2012), vol. 2.